Heliyon 10 (2024) e28698

Contents lists available at ScienceDirect

Heliyon

journal homepage: www.cell.com/heliyon

Research article

Thermal-hydraulic performance and flow phenomenon evaluation of a curved trapezoidal corrugated channel with E-shaped baffles implementing hybrid nanofluid

Rifat Ahamed [a], Musfequs Salehin [b], M Monjurul Ehsan [a,*]

[a] Department of Mechanical and Production Engineering (MPE), Islamic University of Technology (IUT), Gazipur, 1704, Bangladesh
[b] Department of Aerospace Engineering, Bangabandhu Sheikh Mujibur Rahman Aviation and Aerospace University, Dhaka, 1215, Bangladesh

ARTICLE INFO

Keywords:
Heat transfer
Hybrid nanofluid
Curved corrugated
Baffles
Thermal-hydraulic
Vortex generation

ABSTRACT

A numerical investigation of a curved trapezoidal-corrugated channel with E-shaped baffles is conducted for thermal-hydraulic performance and flow behavior involving the use of single and hybrid nanofluids. This investigation introduces a unique integrated methodology for enhancing heat transfer efficiency by simultaneously combining geometric modifications and optimizing coolant utilization. To simulate turbulent, single-phase flow in three-dimensional corrugated channels, a computational model has been developed. The model considers a Reynolds number (Re) range of $5 \times 10^3 \leq Re \leq 35 \times 10^3$ and implies a uniform heat flux of 1000 W/m^2. A commercial software, Ansys fluent was used in order to simulate the fluid flow by setting the inlet temperature at 300 K and velocity according to the Reynolds number. The continuity equation, momentum equation, and energy equations are discretized using a second-order upwind method. The equation's residual has been assigned a value of 1×10^6 for absolute criteria. The study evaluates the thermal-hydraulic performance of single nanofluids (Al_2O_3/water, CuO/water, SiO_2/water) and hybrid nanofluids (Al_2O_3–Cu/water, TiO_2–SiO_2/EG-water) at varying volume fractions ($1\% \leq \varphi \leq 5\%$). Additionally, the investigation examines the effects of corrugations, baffles, and geometric parameter: blockage ratio (BR = 0.10, 0.15, 0.25). The findings demonstrate that the effects of baffles and corrugations can lead to the creation of vortex flow and greater turbulence, which can promote heat transfer enhancement. Various nanofluids demonstrated a significant rise in the Nusselt number, ranging from 35% to 60%, when compared to water in a curved corrugated channel. Additionally, a lower BR resulted in a smaller but still notable gain of 15%–19%. An effective heat exchanger that results in a significant energy dissipation is measured by the energy ratio (ER). The use of corrugated channels with narrow baffles has been found to consistently outperform smooth channels in terms of thermo-hydraulic parameters, leading to enhanced heat transfer. Using BR = 0.10 over 0.25 resulted in an increase in ΔP, HTC, and ER of 48.44%, 18.71%, and 45.86%, respectively. The implementation of a hybrid nanofluid consisting of 1% (20% TiO_2-80% SiO_2)/(60% Water-40% EG) volume fraction in a curved corrugated channel with baffles resulted in a significant improvement of 36.49% in thermal performance. This finding suggests that the aforementioned nanofluid composition and design parameter, characterized by a blockage ratio of 0.10, are the most effective in enhancing thermal performance.

* Corresponding author.
E-mail address: ehsan@iut-dhaka.edu (M.M. Ehsan).

https://doi.org/10.1016/j.heliyon.2024.e28698
Received 7 November 2023; Received in revised form 28 February 2024; Accepted 22 March 2024
Available online 29 March 2024

Nomenclature

g	Acceleration of gravity, $m.s^{-2}$
A	Area, mm^2
BR	Blockage Ratio
X,Y,Z	Cartesian X, Y, Z-coordinate
k	Thermal Conductivity
D	Diameter of corrugation, mm
f_{drag}	Drag function
V_{dr}	Drift velocity, m/s
G	Generation of Turbulent Kinetic energy, Kg/ms^3
HTC	Heat transfer coefficient, (W/m^2. K)
h_b	Height of baffle, mm
H	Height of channel, mm
D_h	Hydraulic diameter, mm
c_1, c_2, C_μ, σ_K, σ_ε	Model constant
$\overrightarrow{a}$	Nanoparticles acceleration, $m.s^{-2}$
Nu	Nusselt number
P	Pitch of corrugation, mm
PEC	Performance evolution criterion
Pr	Prandtl number
p	Pressure, Pa
Δp	Pressure drop, Pa
V_{pf}	Relative velocity, m/s
Re	Reynolds number
C_P	Specific heat capacity (J/Kg.k)
T	Temperature, K
V	Time-mean and fluctuating velocity, m/s
I	Turbulent intensity
k	Turbulent kinetic energy, (m^2/s^2)
u,v,w	Velocity component, m/s
e	Width of baffle, mm
W	Width of tested channel, mm

Greek symbols

μ	Dynamic viscosity of the fluid, kg/m.s
ρ	Density, kg/m^3
σk	Diffusion Prandtl number for k
ε	Turbulent kinetic dissipation, m^2/s^2

Subscripts

av	average
b	baffle
$corr$	corrugated
in	inlet
out	outlet
m	mean
mod	modified
f	fluid
bf	base fluid
nf	nanofluid
hnf	hybrid nanofluid
np	nano particle
ref	smooth pipe
w	wall
s	particles phase

Abbreviations

NF	Nanofluid
HT	Heat transfer
VF	Volume fraction

1. Introduction

High thermal performance is essential for mechanical applications across various industries. Various designs and technology have improved thermal efficiency, leading to advancements in material optimization and reduced physical dimensions and costs. Curved channels are crucial in various applications, including aerospace, astronautics, nuclear reactor design, and cooling. Corrugation design and baffles increases heat transfer rates and reduces thermal resistance, while secondary flow zones enhance fluid mixing and heat transmission [1]. Nanofluid implementation is crucial for improving heat transfer in pipes and channels. Single-phase HT fluids like transformer propylene glycol, oil, ethylene glycol, water, and motor oil are often utilized in thermal power plants, chemical industries, and process industries. However, their low thermal conductivity makes them subpar. Heat transfer intensification can help achieve energy and cost reductions. The current geometry has a great potential on enhancing the heat transfer due to a spectacular geometric configuration. The geometry consists of baffles and corrugation. Trapezoidal corrugation has shown to have better augmentation in heat transfer due to more surface area and recirculation zone. Naphon [2] provides an analysis of the heat transfer properties and pressure drop in a channel featuring V-shaped corrugated upper and lower plates, while maintaining a constant heat flux. The impact of the corrugated surface on the augmentation of heat transfer and pressure reduction is substantial. The channel featuring a corrugated surface exhibits higher heat transmission coefficients compared to the plain surface due to the existence of recirculation zones. Ajeel et al. [3] conduct a numerical simulation to examine the combined effects of nanofluid and various parameter designs on the thermal and hydraulic performance of a house-shaped corrugated channel. The results indicate that a h/W ratio of 0.05, a p/L ratio of 0.075, and an e/r ratio of 0.6667 are the optimal parameters that significantly enhanced thermal performance. Dormohammadi et al. [4] utilized the entropy generation minimization method to optimize fluid flow and heat transfer within a wavy channel. The usage of baffles is a prosperous was to enhance the heat transfer. Lower Heat Transfer Areas (LHTA) formation, especially in the downstream region of baffles, is a challenge associated with baffled channels. Sahel et al. [5] conducted an investigation to ascertain the performance of a perforated baffle consisting of a series of four holes positioned in three distinct locations. In comparison to the conventional baffle, the outcomes indicate that the Pores Axis Ratio (PAR) of 0.190 is the optimal design for substantially eliminating LHTAs, thereby increasing the heat transfer rate by 2%–65%. Maxwell [6] suggested adding solid particles to single-phase fluids, but this could cause sedimentation, blockage, erosion, and increased pressure drop. Alklaibi et al. [7] conducted an experimental investigation on the performance of a flat plate solar collector by circulating nanodiamond nanofluid throughout it under thermosyphon conditions. In order to produce the nanofluids, nanodiamond (ND) nanoparticles were incorporated. The collector thermal efficiency of 69.85% is attained with a 1.0 vol% ND/water nanofluid, representing a 12.7% improvement compared to the efficiency achieved with purified water. Experimentally, Sundar et al. [8] investigated the exergy of the second law for transition flow in a conduit containing a nanodiamond nanofluid composed of a 40:60% (weight) mixture of propylene glycol and water. As a coolant, the study unequivocally demonstrates that the ND nanofluid composed of a mixture of propylene glycol and water exhibits excellent thermal performance, especially in extremely warm regions. According to Sajadi and Kazemi [9], adding a little quantity of TiO_2-water nanoparticles raises HTC. According to Heris et al. [10], The k of the Al_2O_3/water nanofluid produced by the HTC method demonstrates notably elevated values in comparison to those seen in pure water. Awais et al. [11] describes in great depth how the heat transfer and ΔP performance of nanofluids is affected by magnetic fields, working temperatures, compound passive techniques. Saleh and Sundar [12] conduct an experimental evaluation of the thermal performance, embodied energy, and environmental CO2 emissions associated with the passage of water nanofluid and MWCNTs through a double pipe U-bend heat exchanger. The cost of the heat exchanger is decreased from 63 dollars to 61.46 dollars when 0.3 vol percent nanofluid is employed over water. Additionally, an experimental investigation of the flow of nickel/water nanofluid within a corrugated plate heat exchanger is undertaken [13]. The utilization of nanofluids reduces the performance index ratio, as determined by Saleh and Sundar, as a result of the increased viscosity, friction factor, pressure drop, and pumping power.

1.1. Nanofluid for heat transfer enhancement

For a concentration range of 0.1–0.4%, Aliabadi et al. [14] conducted an experiment on forced convective flows of nanofluids via a corrugated wavy channel, revealing superior heat transfer through wavy channels and increased thermal performance with higher volume concentration. According to Noor et al. [15], when an Al_2O_3/water nanofluid flows via corrugated channels, heat transmission is improved by around 10.5%–50.15% when compared to water. Wen and Ding [16] studied the properties of heat transfer in a tube under laminar flow and found a 47% improvement in heat transfer efficiency at a volume percentage of 1.6% using an Al_2O_3/water nanofluid. This improvement was observed in contrast to the base fluid, which consisted only of water. Ahmed et al. [17] has identified the most effective nanofluid in the rectangular corrugated minichannel with an amplitude-to-wavelength ratio of 0.12 to be 3% Al2O3–CuO/water. Akbarinia and Laur [18] have quantitatively examined the impact of the diameter of the nanoparticle on laminar mixed convection flow in a circular curved tube. The results show that when the diameter of the nanoparticle increases, the Nusselt number and secondary flow drop. With a relative surface roughness of 0.003, Ehsan et al. [19] has shown that Al2O3-water has a better heat transfer characteristics when the VF is set to 2% which led to a minimum pumping power.

1.2. Passive heat transfer enhancement techniques using nanofluid

There are a few parameters which influence the HT rate. Lots of researchers have been trying to change the fluid characteristics and fluid domain to acquire the best HT rate. To improve heat and mass transfer, Scott and Lobato [20] developed a cross-corrugated triangular/sinusoidal duct for plate heat exchangers. The thermo-hydraulic properties of turbulent nanofluid flow in various

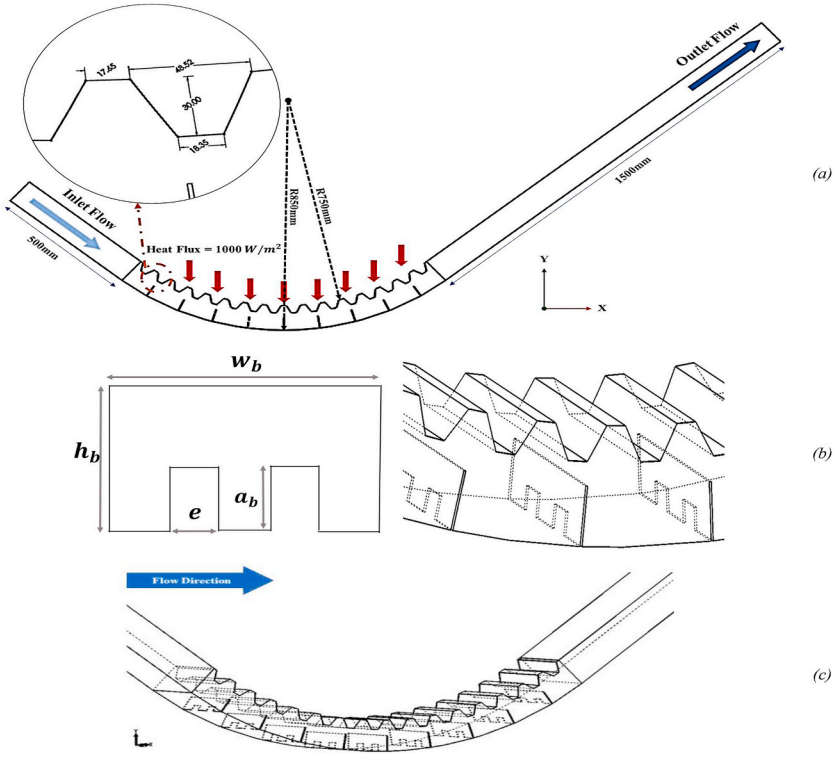

Fig. 1. Computational domain's schematic illustration: (a) Geometry and measurements of the model, (b) Baffle configuration, (c) Baffle position along the flow direction.

Table 1
Channel's geometric structure with baffles.

Parameters	Terminology	Value (mm)
Horizontal length of channel	L	3200
Width of channel	W	200
Vertical height of channel	H	100
Hydraulic diameter	D_h	133.33
Baffle thickness	t	2
Horizontal baffle width	w_b	200
Vertical baffle height	h_b	50
Blockage ratio	$BR\ (e/w_b)$	0.10, 0.15, 0.25

corrugated channel types were studied by Ajeel et al. [21]. The findings demonstrated that, in comparison to straight and zigzag channels, the trapezoidal channel has a greater impact on thermal efficiency. Afterwards, Ajeel et al. [22] used SiO_2-water to study the impact of geometrical factors on the thermo-hydraulic properties of a trapezoidal-corrugated channel. The obtained data demonstrated that at a Re of 30,000, the rise of *Nu* was 99.45% with an increase in the (h/W) ratio from 0.0 to 0.05. Research on the improvement of nanofluid heat transfer under turbulent flow in a straight channel was carried out by Abdolbaqi et al. [23] using TiO_2 and CuO at different volume concentration. They discovered that when volume fractions grew, the Nusselt number and wall shear stress also increased, suggesting that nanofluids have a great deal of promise to improve heat transmission. Ehsan et al. [24] has brought a numerical investigation using 3 different types of nanofluid where the lowest thermos hydraulic characteristics was observed with the usage of CuO-water. According to research by Noor et al. [25], the ideal working substance is 3% of all nanofluids since at this VF, the pumping power needed is lowest for all HTC values.

Laminar forced convection has been statistically investigated by Santra et al. [26] for CuO-water NF between two parallel plates. The rate of heat transfer has been demonstrated to rise in proportion to increases in Re and nanoparticle volume concentrations. The HT properties of Al_2O_3-water NF flow in a triangular minichannel with continuous heat flux were investigated by Bahiraei and Majd [27]. According to Nakhchi and Esfahani [28], utilizing Cu-water nanofluid flow inside perforated conical rings at a VF of 1.5% yields the highest thermal performance of 1.10. The flow of a copper-water nanofluid in a tube and its heat transfer were experimentally investigated by Xuan and Li [29]. They found that when the concentration of solid particles rose, so did the improvement in transfer of

heat. In ribbed channels, both Manca et al. [30] and Mohammed et al. [31] conducted numerical studies on the flow and heat transmission of nanofluid. The findings showed that when Re and VF of nanoparticles increased, the improvement in heat transfer also increased, although at the expense of a higher pressure drop. The numerical evaluation carried out by Awais et al. [32] yields significant ideal findings for achieving the desired thermo-hydraulic performance of the serpentine tube heat exchanger.

1.3. Corrugated channel with baffles

Implementation of baffles has become a promising way to escalate the heat transfer enhancement (HTE). Lots of researchers have studied with different sizes and shapes of baffles to demonstrate a more effective solution. An improved definition of drag reduction, taking into account turbulence effects, yields the same amount of drag reduction in both coiled and straight pipes, according to a study on drag-reducing flow in curved pipes by Gasljevic and Matthys [33]. There was a noticeable decrease in drag for bigger welded elbows, and roughly 40% less for smooth elbows. In a study conducted by Noorani et al. [34], mentioned that a pipe's curvature produces centrifugal forces, which cause the mean axial flow to go to the bent pipe's outer side. Secondary motion perpendicular to the original flow may arise from this. Strongly curved pipes exhibit a clear slope shift below the pipe's center due to the noticeable bulge in secondary flow, which alters the mean axial velocity. In order to study the bend of a pipe, Yang and Chiang [35] did an experimental analysis to study the heat transfer for periodically varying-curvature curved-pipe. He claimed that the performance of a heat exchanger or solar collector can be improved by using S-shaped pipes rather than straight pipes. The impact of baffle turbulators on HTE was examined by Sriromreun et al. [36] using computational and experimental methods utilizing a rectangular channel. As compared to a smooth channel, their results showed that the Z-baffle's presence significantly affected the HTE. Promvonge et al. [37] quantitatively studied laminar flow in a baffled channel for several pitch ratios and blockage ratios and found that a 30° angled baffle provides a beneficial boost for the HT rate. Noor et al. [38] has conducted an experiment using V shaped Corrugated tube and observed that nanofluid with 3% volume fraction has 40% lower Friction factor compared to water. HT characteristics were analyzed numerically and experimentally by Nanan et al. [39] employing baffles in circular tubes. The experiments concentrated on a number of characteristics, including baffle twist ratios and width ratios spanning the range of Re from 6000 to 20,000. The results demonstrated that, in comparison to the other investigated ratios, the transverse twisted baffles with the shortest twist ratio recorded a better thermal performance evolution criterion (PEC). The baffle inclination effect in a rectangular channel was investigated experimentally and computationally by Lu and Jiang [40]. Several baffle forms were presented by Kamali and Binesh [41] to increase the cooling degree in the gas turbine. After analyzing several forms, they came to the conclusion that the trapezoidal baffle shape is the optimum option for improving HT and reducing pressure. According to Ahmed et al. [42], the best-performing hybrid nanofluid in the double-dimpled pipe flow was found to be 3% Al2O3–CuO/water, with a maximum thermal performance improvement of 20.62%. The introduction of baffles in fluid flow had become one prosperous way of enhancing the heat transfer rate. But still one issue arises when complex geometries are introduced for manufacturing. The manufacturing cost for a bulk production should have a profit limit in order to cause a significance in practical fields. Jian et al. [43] introduced some complex design of baffles which causes a great augmentation in the heat transfer. Bichkar et al. [44] also introduced some baffles for shell and tube heat exchanger. In term of manufacturing complexity, different types of microchannels are being manufactured in a bulk production which are heavily used. Hussein [45] mentioned different complex shaped multi-mini-channel heat sink. Various Fin design for conjugate heat transfer optimization in double pipe are mentioned by Iqbal et al. [46] having difficult design of modeling them. The method of modeling Micro-Channel Geometric Features through Abrasive-Assisted Electrochemical Jet Machining was proposed by Gao et al. [47] which can reduce manufacturing cost and time. Fabrication of complex multilevel microchannels in PDMS by using three-dimensional photoresist masters was done by Yun and Yoon [48]. Compared to all the aforementioned geometries, the current geometry has better prosperity in the field of manufacturing and heat transfer.

1.4. Features of hybrid nanofluid

Researchers are utilizing hybrid nanofluid to enhance the fluid's properties, a significant advancement in heat transfer mechanisms. The literature papers provide an overview of the primary research conducted in recent years on the measurement of thermal conductivity in single and hybrid nanofluids. According to Awais et al. [49], compared to a single-step process, the two-step method of nanofluid production has been determined to be the most cost-effective. Bhattacharya et al. [50] experimentally established thermophysical characteristics of porous metal foams, including permeability, inertial coefficient, and effective thermal conductivity. They developed an analytical model using hexagonal ligaments and large connections. Das et al. [51] studied thermal conductivity enhancement by inserting 38 nm-sized alumina oxide nanoparticles into water, revealing a 24.3% improvement at higher temperatures and volume concentrations. The synthesis of silicon dioxide (SiO_2) coated on magnetite (Fe_3O_4) particle doped multi-walled carbon nanotubes (MWCNTs) (Fe_3O_4@SiO_2/MWCNTs) hybrid nanoparticles was done by Baby and Sundara [52] using a straightforward chemical reduction approach. Vinoth et al. [53] investigates the heat transfer characteristics of a microchannel heat sink with an oblique finned curve, employing various working fluids such as Al_2O_3+CuO/water, deionized water, and Al_2O_3/water. The heat transfer rate, PEC, and pressure drop of the curved MCHS are 30.1% higher than those of the straight channel heat sink due to the usage of hybrid nanofluid. Sundar et al. [54] conducted an experiment to determine the thermal conductivity of an Al_2O_3 nanoparticle-based mixed base fluid. The fluids were a 20:80, 40:60, and 60:40 combination of ethylene glycol and water. The study found that the nanofluid with 20:80 EG: water at 60 °C and 1.5% volume concentration had a higher thermal conductivity of around 32.26% than the base fluid. Pazarlıoğlu et al. [55] carried out an investigation on a parabolic trough collector receiver tube containing elliptical dimpled fins with different elliptical ratios under turbulent flow regime using 2.0 %TiO_2/Syltherm800, 2.0 %Al_2O_3/Syltherm800, 0.5

Table 2
Empirical constant for turbulent model.

Empirical Constant	Value
$\mu_{t,m}$	$\rho_m C_\mu \frac{K^2}{\varepsilon}$
C_1	1.44
C_2	1.92
C_μ	0.09
σ_k	1
σ_ε	1.3

% TiO_2-1.5 % Al_2O_3/Syltherm800, 1.0 % TiO_2-1.0 % Al_2O_3/Syltherm800, and 1.5 % TiO_2-0.5 % Al_2O_3/Syltherm800. In an experiment, Soltani and Akbari [56] investigated the viscosity of a MgO-MWCNT hybrid nanofluid based on ethylene glycol. The effect of increasing nanofluid concentration on viscosity was shown to follow a nonlinear pattern, with lower concentrations having less of an impact. From the base fluid to the 1% concentration, the research observed a total increase in viscosity of 168%, showing a considerable rise in effective fluid dynamic viscosity. Moldoveanu et al. [57] used pure water to suspend Al_2O_3 and TiO_2 nanoparticles individually and then combined them as a combination (Al_2O_3–TiO_2) to measure the hybrid and nanofluids' viscosity. Al_2O_3–CuO/water hybrid NF's performance in electronic heat sinks was evaluated by Selvakumar and Suresh [58]. The researchers reached the conclusion that the use of nanofluid resulted in a 24.35% increment in HT. A study that investigated the numerical modeling of hybrid nanofluid with gold and silver nanoparticles across a stenotic artery by Waqas et al. [59] The study found gold and silver as nanoparticles are effective in reducing stenosis hemodynamics. Using ternary hybrid nanofluid Zn:Ag:Co/EG-H_2O with a 1% volume fraction in a two-dimensional pipe under turbulent flow conditions, Ekiciler [60] conducted an extremely fascinating investigation. According to the study, Zn:Ag:Co/EG- H_2O hybrid nanofluid conveyed in a pipe with increasing wall corrugation exhibited the highest efficiency.

1.5. Research scope and problem statement

The power generation, manufacturing sector, refrigeration, electronics, recovery of waste heat, space applications, air conditioning, chemical and food industries and environment engineering are just a few of the industries who rely significantly on curved channels. Therefore, this study presents a numerical investigation that provides a corrugated channel to examine the flow behavior and HT properties of various NF alongside hybrid nanofluid, utilizing the single-phase mixture approach. Curved corrugated channels, often with baffles, are used in various industries to enhance heat transfer efficiency. Curved corrugated channels with baffles improve heat transfer efficiency in industry sectors such as heat exchangers, HVAC systems, and chemical processes. These channels disturb fluid flow, increasing turbulence, which enhances fluid mixing and decreases the thickness of the boundary layer, allowing for more efficient heat exchange. They also overcome physical and geometrical limits by enabling for compact designs with high heat transfer rates in a small footprint, allowing space constraints to be overcome while maintaining heat transfer performance. Increasing the surface area for HT and promote turbulence, enhancing overall efficiency in heat exchangers. These channels are also used in chemical reactors to improve reactant mixing efficiency. They are also used in cooling systems, such as autos and electrical gadgets. They are also used in aircraft heat exchangers to regulate thermal loads and maintain appropriate temperatures. They are also used in rocket engines' cooling systems. Solar thermal collectors use curved corrugated tubes with baffles to capture and transport solar energy. In order to increase the effectiveness and viability of renewable energy sources, these channels are also utilized in ocean thermal and geothermal energy conversion systems. They are also used in nuclear reactor cooling systems to regulate heat transfer processes and maintain operational safety. Industries with significant waste heat generation, such as steel production or power plants, use these channels to recover and repurpose thermal energy, thereby improving overall energy efficiency.

Research on the impact of coolants and surfaces on heat exchanger performance is crucial for superior design. This paper proposes a comprehensive approach combining coolant optimization and geometry correction for optimal heat transfer. The study highlights the lack of research on evaluating hybrid nanofluids in E-shaped trapezoidal curved corrugated pipes and proposes the use of an E-shaped pipe to improve heat transfer efficiency. The usage of different types of nanofluid may result in enhanced HT but the usage of hybrid nanofluid can double the outcome which was the core target of the research. The flow behavior can be altered due to the presence of baffles and corrugation for different thermo-hydraulic parameters which is broadly described. The present study also considers variations in the magnitude of velocity for ΔP, HTC, friction factor, *Nu*, enhancement ratio, and friction ratio. This work aims to assess the performance of hybrid nanofluids, namely the Al_2O_3–Cu/water and 20% TiO_2-80% SiO_2/EG-water mixtures, as well as nanofluids consisting of CuO/water, Al_2O_3/water, and SiO_2/water. The evaluation is conducted via the use of computational approaches. In order to assess the optimal thermal performance, this study examines the impact of varying VF and ReThe findings of this study possess the potential to provide valuable insights for future research attempts aimed at improving and optimizing the heat transfer efficiency of corrugated channel designs.

Table 3
Numerical Data for boundary conditions.

Density	Thermal Conductivity	Cp	Viscosity	Reynolds Number	Hydraulic Diameter	Velocity	Intensity
996	0.615	4178	0.000798	5000	0.13333	0.030046	5.517
996	0.615	4178	0.000798	10000	0.13333	0.060092	5.059
996	0.615	4178	0.000798	15000	0.13333	0.090138	4.809
996	0.615	4178	0.000798	20000	0.13333	0.120184	4.639
996	0.615	4178	0.000798	25000	0.13333	0.15023	4.512
996	0.615	4178	0.000798	30000	0.13333	0.180276	4.410
996	0.615	4178	0.000798	35000	0.13333	0.210322	4.326

2. Materials and methods

2.1. Physical model

Fig. 1 displays a schematic representation of the study model, which features a curved trapezoidal corrugated channel design. The structure comprises of two distinct walls, notably a top wall with a corrugated surface and a lower wall with a smooth surface. The vertical distance separating the upper and lower walls measures 0.1 m, while the channel's width and horizontal length, in relation to the corrugated wall, are 0.2 m and 1.2 m, respectively. Table 1 presents a comprehensive depiction of the geometric configuration of the channel.

The present study has been conducted using 2 cases.

- The variation of thermophysical properties due to the implementation of nanofluid (CuO/water, SiO_2/water, Al_2O_3/water) and hybrid nanofluid (Al_2O_3–Cu/water, TiO_2–SiO_2/EG-water) as working fluid for a range of $5000 \leq Re \leq 35{,}000$.
- The investigation of flow behavior in the curved corrugated channel involves the utilization of various blockage ratios (BR = 0.10, 0.15, 0.25).

2.2. Mathematical modelling

Equations that characterize fluid motion are called Navier-Stokes equations. Initially the Continuity equation which asserts that a fluid's mass inside a specific volume must remain constant throughout a period employed to derive the Navier-Stokes equation as stated in Eqn. (1).

$$\nabla(\rho.\mathrm{u}) = 0 \tag{1}$$

It can be written in the format of;

$$\rho\left(\frac{\partial u}{\partial x}+\frac{\partial v}{\partial y}+\frac{\partial w}{\partial z}\right)=0 \tag{2}$$

Applying the concept of conservation of momentum which asserts that the change in a fluid's momentum inside a certain volume equals the net force applied the momentum equation explains the forces acting on a fluid and how they affect its motion. An incompressible fluid's momentum equation is provided by:

$$(\mathrm{u}\cdot\nabla)\mathrm{u} = -\frac{1}{\rho}\nabla p + \nu\nabla^2\mathrm{u} \tag{3}$$

The fluid's momentum change rate is represented by the left, while the net force is represented by the right. The viscous force, pressure gradient force and the impact of temperature and pressure changes on density are represented by the terms.

The Momentum Equation can be derived in a form of,

$$\rho\left(u\frac{\partial u}{\partial x}+v\frac{\partial u}{\partial y}+w\frac{\partial u}{\partial z}\right)=\frac{\partial}{\partial x}\left(\mu\frac{\partial u}{\partial x}\right)+\frac{\partial}{\partial y}\left(\mu\frac{\partial u}{\partial y}\right)+\frac{\partial}{\partial z}\left(\mu\frac{\partial u}{\partial z}\right)-\frac{\partial p}{\partial x} \tag{4}$$

$$\rho\left(u\frac{\partial v}{\partial x}+v\frac{\partial v}{\partial y}+w\frac{\partial v}{\partial z}\right)=\frac{\partial}{\partial x}\left(\mu\frac{\partial v}{\partial x}\right)+\frac{\partial}{\partial y}\left(\mu\frac{\partial v}{\partial y}\right)+\frac{\partial}{\partial z}\left(\mu\frac{\partial v}{\partial z}\right)-\frac{\partial p}{\partial y} \tag{5}$$

$$\rho\left(u\frac{\partial w}{\partial x}+v\frac{\partial w}{\partial y}+w\frac{\partial w}{\partial z}\right)=\frac{\partial}{\partial x}\left(\mu\frac{\partial w}{\partial x}\right)+\frac{\partial}{\partial y}\left(\mu\frac{\partial w}{\partial y}\right)+\frac{\partial}{\partial z}\left(\mu\frac{\partial w}{\partial z}\right)-\frac{\partial p}{\partial z} \tag{6}$$

The energy equation is finally derived. It stipulates that the heat supplied to a fluid, along with the work the fluid does on its surroundings, must equal the rate of change in internal energy of the fluid within a constant volume.

$$\rho\left(\mathrm{u}\frac{\partial T}{\partial x}+v\frac{\partial T}{\partial y}+w\frac{\partial T}{\partial Z}\right)=\frac{\partial}{\partial x}\left(\frac{k_f\partial T}{C_p\partial x}\right)+\frac{\partial}{\partial y}\left(\frac{k_f\partial T}{C_p\partial y}\right)+\frac{\partial}{\partial z}\left(\frac{k_f\partial T}{C_p\partial z}\right) \tag{7}$$

Table 4
Thermo-hydraulic Parameter data set for 1% VF Al_2O_3/water.

Reynolds Number	Hydraulic Diameter (mm)	Mean Temperature (k)	Mass Flow Rate	Heat Transfer coefficient	Nusselt number	Friction factor	Pressure Drop (Pa)	PEC	Enhancement ratio	Friction Ratio	Energy ratio
5000	0.13333	300.0661	0.44954157	297.5786	62.69991	0.168775	32.788	1.8218	2.70112	3.2593	35.7122
10000	0.13333	300.0711	0.89908315	535.4388	112.8171	0.129003	118.992	2.5743	3.44533	2.3973	61.2067
15000	0.13333	300.0724	1.34862472	753.6938	158.8036	0.114438	257.653	2.6571	3.56118	2.4074	84.5183
20000	0.13333	300.0776	1.79816630	954.4895	201.1113	0.106999	451.608	2.7379	3.68115	2.4304	106.2800
25000	0.13333	300.0824	2.24770787	1164.759	245.4152	0.102402	701.964	2.8045	3.78458	2.4575	129.3549
30000	0.13333	300.0856	2.69724945	1376.71	290.0733	0.099702	1012.191	2.8331	3.84140	2.4928	152.9966
35000	0.13333	300.0918	3.14679102	1588.298	334.655	0.097486	1373.429	2.8504	3.87460	2.5117	176.2368

Table 5
Thermo-hydraulic Parameter data set for 1% VF TiO_2–SiO_2/Water-EG.

Reynolds Number	Hydraulic Diametre (mm)	Mean Temperature (k)	Mass Flow Rate	Heat Transfer coefficient	Nusselt number	Friction factor	Pressure Drop (Pa)	PEC	Enhancement ratio	Friction Ratio	Energy ratio
5000	0.13333	300.0725	1.38750089	328.5962	96.26412	0.17164	298.681	2.7814	4.14707	3.3146	54.789
10000	0.13333	300.0768	2.77500179	597.9829	175.1825	0.13221	1081.592	3.9648	5.35004	2.4570	94.867
15000	0.13333	300.0802	4.16250268	846.7644	248.0645	0.11725	2345.915	4.1173	5.56299	2.4666	131.893
20000	0.13333	300.084	5.55000358	1093.332	320.2979	0.10971	4121.168	4.3244	5.86276	2.4919	169.288
25000	0.13333	300.0889	6.93750447	1340.111	392.5932	0.10505	6405.155	4.4484	6.05425	2.5210	206.948
30000	0.13333	300.0925	8.32500537	1588.695	465.4171	0.10181	9190.886	4.5141	6.16344	2.5454	244.902
35000	0.13333	300.0992	9.71250626	1838.993	538.7434	0.09934	12501.658	4.5599	6.23751	2.5596	283.394

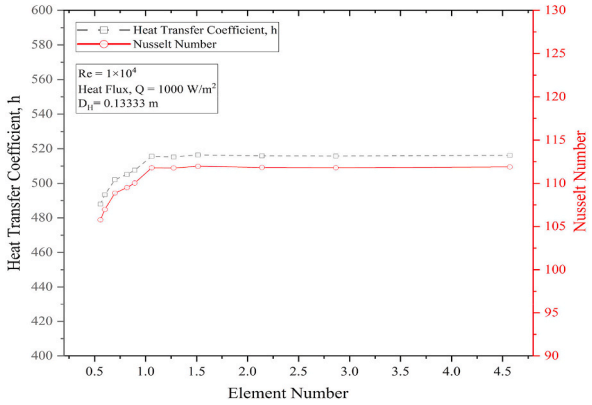

Fig. 2. Grid independency test.

Shortly written as;

$$\nabla.(\mathrm{e}u) = \nabla.(k\nabla \mathrm{T}) + \mathrm{Q} \tag{8}$$

The Volume fraction Equation can be derived as;

$$\frac{\partial}{\partial x}\left(\varphi_p \rho_p u_m\right) + \frac{\partial}{\partial y}\left(\varphi_p \rho_p v_m\right) + \frac{\partial}{\partial z}\left(\varphi_p \rho_p w_m\right) = -\frac{\partial}{\partial x}\left[\varphi_p \rho_p u_{dr,p}\right] - \frac{\partial}{\partial y}\left[\varphi_p \rho_p v_{dr,p}\right] - \frac{\partial}{\partial z}\left[\varphi_p \rho_p w_{dr,p}\right] \tag{9}$$

Thermal conductivity can be defined by;

$$k_m = \sum_{s=1}^{n} \varphi_s k_s \tag{10}$$

Density can be defined by;

$$\rho_m = \sum_{s=1}^{n} \varphi_s \rho_s \tag{11}$$

Viscosity can be defined by;

$$\mu_m = \sum_{s=1}^{n} \varphi_s \mu_s \tag{12}$$

Mass average velocity is written as:

$$\overrightarrow{V_m} = \frac{1}{\rho_m} \sum_{x=1}^{n} \varphi_s \rho_s \overrightarrow{V_s} \tag{13}$$

The expression for the drift velocity of particles formulated as:

$$\overrightarrow{V_{dr,s}} = \overrightarrow{V_s} - \overrightarrow{V_m} \tag{14}$$

For the model validation, Launder and Spalding k–ε turbulence model is used and derived by the following equations. The empirical constants of the k–ε turbulence model are presented in Table 2.

$$\nabla(\rho_m V k) = \nabla\left(\frac{\mu_{t,m}}{\sigma_k}\nabla \mathrm{k}\right) + G_m - \rho_m \varepsilon \tag{15}$$

$$\nabla(\rho_m V \varepsilon) = \nabla\left(\frac{\mu_{t,m}}{\sigma_\varepsilon}\nabla \varepsilon\right) + \frac{\varepsilon}{k}(C_1 G_m - C_2 \rho_m \varepsilon) \tag{16}$$

2.3. Boundary conditions

At the intake border the flow velocity was set according to the Reynolds number and the inlet temperature was set as 300 K. The Turbulence intensity was set as 5.517% in the Ansys model setup for a medium turbulence case in the model setup according to the corresponding Reynolds number. There is a no-slip boundary condition on the channel's wall. The equations presented below provide the boundary conditions that are relevant to the channels that were examined in the present investigation.

Inlet boundary:

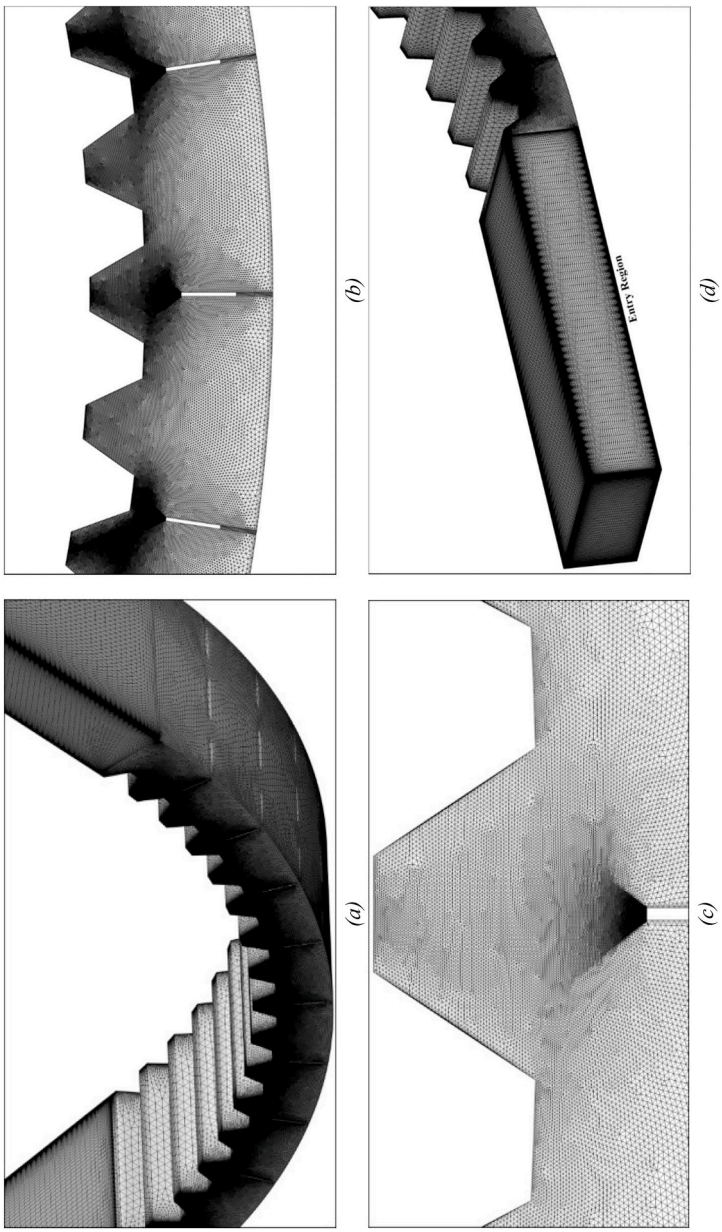

Fig. 3. Mesh structure along the length and at the cross section of the channel.

Table 6
Mesh convergence study.

Cell Number	Nusselt Number	HTC	%Error in *Nu*
557370	105.77468	487.89792	–
600400	106.96921	493.40782	−1.1167%
699150	108.86109	502.13435	−1.7378%
817620	109.52479	505.19572	−0.606%
892660	110.0386	507.56571	−0.4669%
1060640	111.79526	515.66854	−1.5713%
1275170	**111.78292**	**515.25036**	**0.01104%**
1513590	111.96217	516.4384	−0.1601%
2141110	111.83591	515.85605	0.1129%
2864740	111.81154	515.74364	0.0218%
4570270	111.89408	516.12434	−0.0738%

$$u = u_{in}, v = w = 0 \tag{17}$$

$$k_{in} = \frac{3}{2}(I\ u_{in})^2, \varepsilon_{in} = C_{\mu}^{\ 3/4}\ \frac{K^{3/2}}{Lt} \tag{18}$$

Outlet boundary:

$$\frac{\partial T_f}{\partial x} = 0, \frac{\partial u}{\partial x} = \frac{\partial v}{\partial x} = \frac{\partial w}{\partial x} = 0, \frac{\partial k}{\partial x} = \frac{\partial \varepsilon}{\partial x} = 0 \tag{19}$$

At the symmetry wall:

$$\frac{\partial v}{\partial x} = \frac{\partial w}{\partial x} = 0, \frac{\partial T}{\partial x} = 0, u = 0 \tag{20}$$

At the upper wall:

$$u = v = w = 0, \mathrm{q} = \mathrm{q_{wal}l} \tag{21}$$

The following presumptions have guided the computations of the numerical simulation.

- A three-dimensional steady state flow with fully developed conditions is seen.
- The importance of natural convection is minimal.
- The gravitational pull may be deemed negligible.
- Uniform velocity at inlet of the pipe
- Quantity of thermal energy dissipated to the surrounding environment is neglected.
- The stability and temperature independence of the thermophysical characteristics of hybrid nanofluids have been observed.

The Boundary conditions applied for the geometry is given in Table 3 below as water being used as a working fluid.

2.4. Performance parameters and dimensionless numbers

The hydraulic diameter is a fundamental parameter used in fluid mechanics to quantify the flow geometry, taking into consideration both the cross-sectional area and perimeter. It can be expressed as [61]:

$$D_h = \frac{2WH}{W + H} \tag{22}$$

The hydraulic diameter may be used to express the Reynolds number as follows [62]:

$$Re = \frac{\rho v D_h}{\mu} \tag{23}$$

The thermophysical characteristics of a fluid are determined by considering its bulk mean temperature (T_m). Eqn. (24) represents the bulk mean temperature [63]:

$$T_m = \frac{T_{in} + T_{out}}{2} \tag{24}$$

Amount of heat transferred can be calculated using [64];

$$\dot{Q} = \dot{m} c_p (T_{out} - T_{\mathrm{in}}) \tag{25}$$

Using $\dot{Q}$, the HTC can be calculated [65]:

Table 7
Base fluid and nanoparticle's properties.

Material	Density, ρ (kg/m^3)	Thermal Conductivity, K (W/mK)	Heat Capacity, C_p (J/kgK)	Dynamic Viscosity, μ (kg/ms) $\times 10^{-3}$
H_2O	995.70	0.615	4178	0.80
SiO_2	2200	1.38	703	–
Al_2O_3	3970	40.0	765	–
CuO	6510	18.0	540	–
TiO_2	4250	8.945	686	–

Table 8
Water-based nanofluid's thermophysical properties for $\varphi = 1\%$ [77].

Nanofluid	Density, ρ (kg/m^3)	Thermal Conductivity, K (W/mK)	Heat Capacity, C_p (J/kgK)	Dynamic Viscosity, μ (kg/ms) $\times 10^{-3}$
SiO_2	1007.743	0.61945	4102.137	0.8203
Al_2O_3	1025.443	0.63279	4045.865	0.8203
CuO	1050.843	0.63183	3952.624	0.8203
0.02(Al_2O_3–Cu)/0.98 Water	1049.25	0.68565	3958.623	1.94
20% TiO_2-80% SiO_2/60% Water- 40% EG	1071.08	0.45512	3469.3319	2.65

$$\dot{Q} = hA_c\Delta T_c \rightarrow h = \frac{\dot{Q}}{A_c\Delta T_c} \tag{26}$$

Friction factor (f) and Nusselt number (Nu) may be calculated as follows [66,67].

$$Nu = \frac{h_{av}D_h}{k} \tag{27}$$

$$f = \frac{2\Delta PD}{\rho v^2 L} \tag{28}$$

For the flow caricaturists on a nanofluid, pressure drop is a necessary parameter. Eqn. (29) represents the pressure drop:

$$\Delta P = P_{\text{in}} - P_{\text{out}} \tag{29}$$

The Performance Evolution Criterion (PEC) is a metric used to assess the efficiency of a heat exchanger in HT, considering fluid flow properties and process characteristics [68]. In comparison to a smooth channel filled with water, it assesses the modified system with a curved corrugated channel.

$$PEC = \frac{Nu_{\text{enhanced}}/Nu_{bf}}{\left(f_{\text{enhanced}}/f_{bf}\right)^{1/3}} \tag{30}$$

The enhancement ratio, which is a performance measure associated with heat transfer, can be defined as:

$$Enhancement\ ratio = \frac{Nu_{mod}}{Nu_{ref}} \tag{31}$$

Additionally, the friction ratio, which is a performance characteristic associated with friction loss, could be mathematically represented with Eqn. (32).

$$Friction\ ratio = \frac{f_{mod}}{f_{ref}} \tag{32}$$

The corresponding data found from Eqn. (22)–(32) has been shown in Table 4 and Table 5 for both Al_2O_3/water and TiO_2–SiO_2/Water-EG of 1% volume fraction.

3. Numerical implementation

This study investigates the heat transfer and flow properties of a curved trapezoidal corrugated channel through the utilization of a numerical simulation method that incorporates nanofluid. The finite volume method is employed in the solution of the governing equations using ANSYS-FLUENT, a commercial computational fluid dynamics (CFD) software. The study utilizes computational methods to solve for turbulent flow in smooth and corrugated pipes, specifically focusing on three-dimensional, single-phase flow. The k-epsilon turbulence model is employed in this analysis. Furthermore, a steady heat flux of 1000 kW/m^2 is employed to the walls with corrugations, whereas no heat transfer occurs to the other walls that are considered smooth. For pressure-velocity coupling, the SIMPLE method is used, and an implicit solver is used to solve the governing equations. Using a second-order upwind method, the

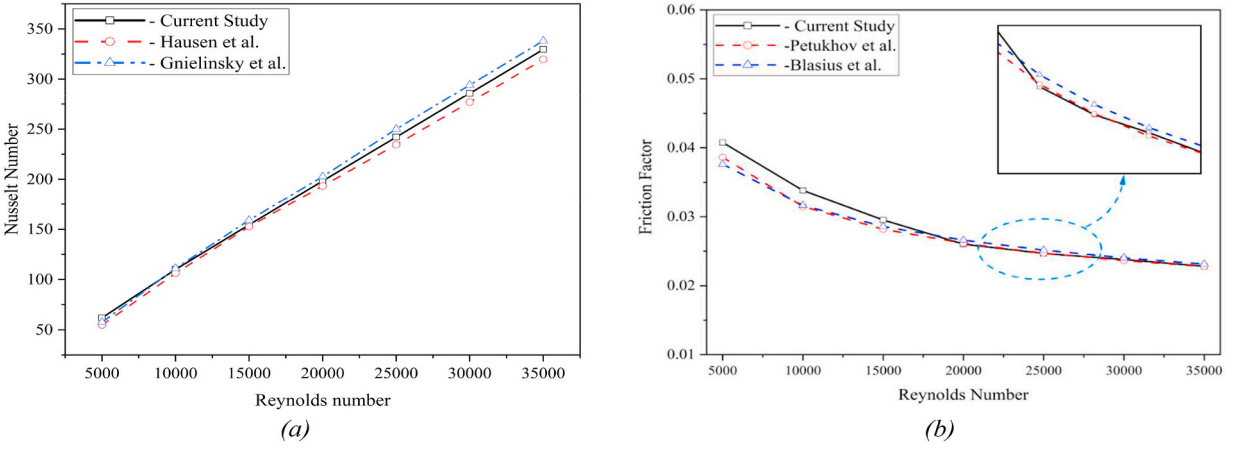

Fig. 4. Comparing the current work's results with the pertinent correlation (a) Nusselt number vs Re for corrugated pipe (b) friction factor vs Re for smooth pipe.

Table 9
Nusselt Number deviation from correlation for present study.

Reynolds Number	Current Study	Gnielinsky Correlation	% Error
5000	61.90245	57.58701	7.4937
10000	110.0386	111.07655	0.9344
15000	154.4729	159.03779	2.8703
20000	198.3685	202.83738	2.2031
25000	242.1579	250.09132	3.1722
30000	285.8221	294.1497	2.8310
35000	329.639	338.23754	2.5421

continuity equation, momentum equation, and energy equations are discretized. A value of 1×10^6 has been assigned to the equation's residual for absolute criteria. The test section is placed 500 mm from the intake to create a zone of fully developed flow in order to evaluate the hydrodynamic properties. Measurements of pressure and temperature are obtained at the initial and final locations within the corrugated region, and these data points are documented during the manipulation of the boundary inlet velocity for a range of 5000–35000 Reynolds number.

3.1. Mesh generation and grid independence analysis

In order to precisely represent the flow properties of channels, a computational domain model incorporating baffles and corrugations is developed to build a steady-state model. The process outlined above is of great significance in the field of numerical calculations, as it has a substantial impact on both computing efficiency and accuracy. The flow characteristics of channels including baffles and corrugations in close proximity to the surface have a substantial impact on both the *Nu* and ΔP. The generation of flow in the mesh is crucial for ensuring precision. The computational domain is meshed using the unstructured tetrahedral element, as depicted in Fig. 3. To get a desired Y+ value of 1, the 1st layer thickness was set to 5.027×10^{-4}. After a cell number of 1275170, the deviation of the Nusselt number turns to less than 1% indicating even if the cell number is increased, the *Nu* number value will not have a high variation shown in Fig. 2. The optimum cell number is set to 1275170 to get the maximum possible result from the simulation with less amount of computational time. Detailed information is mentioned in Table 6.

3.2. Thermophysical properties of nanofluids

Recent studies have provided significant information on the thermophysical characteristics of nanofluids, which are becoming increasingly common in cooling applications. The density of Al_2O_3 and other nanofluids is determined by Vajjha et al. [69] using an Anton Paar digital density metre. A correlation was observed throughout the experimental findings and the mathematical model proposed by Pak and Cho [70].

$$\rho_{nf} = (1-\varphi)\rho_{bf} + \varphi\rho_s \tag{33}$$

The density of hybrid NF was estimated by applying the correlation given by Takabi and Shokouhmand [71]:

$$\rho_{hnf} = (1-\varphi)\rho_{bf} + \varphi_{s,1\rho 1} + \varphi_{s,2\rho 2} \tag{34}$$

A new variable was added as by Rea et al. [72] donated by volume fraction (φ) of nanofluid:

$$\varphi = \frac{V_s}{V_{bf}} \tag{35}$$

Additionally, the following equations, represents the volume fractions:

$$\varphi_{s,1} = \frac{V_{s,1}}{V_{bf}}, \varphi_{s,2} = \frac{V_{s,2}}{V_{bf}} \tag{36}$$

Nanofluid's $c_{p_{nf}}$ can be obtained from the following equation [73];

$$c_{p_{nf}} = \frac{(1-\varphi)\rho_{bf}c_{p_{bf}} + \varphi\rho_s c_{p_s}}{\rho_{nf}} \tag{37}$$

Specific heat of hybrid nanofluid was determined;

$$c_{p,hnf} = \frac{(1-\varphi)\rho_{bf}c_{p_{bf}} + \varphi_{s,1}\rho_1 c_{p,1} + \varphi_{s,2}\rho_2 c_{p,2}}{\rho_{hnf}} \tag{38}$$

Utilizing the Brinkman equation, the dynamic viscosity was obtained as follow [74]:

$$\mu_{nf} = \frac{\mu_{bf}}{(1-\varphi)^{2.5}} \tag{39}$$

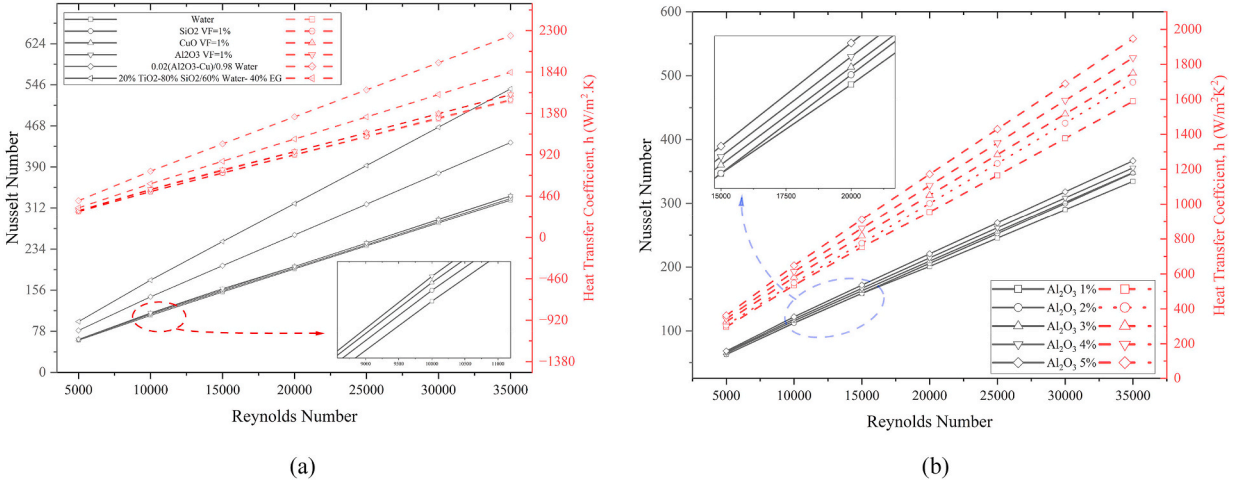

Fig. 5. *Nu* and HTC Variations with Re for (a) utilizing different nanofluid and hybrid nanofluid (b) utilizing 1%–5% volume concentration of Al_2O_3.

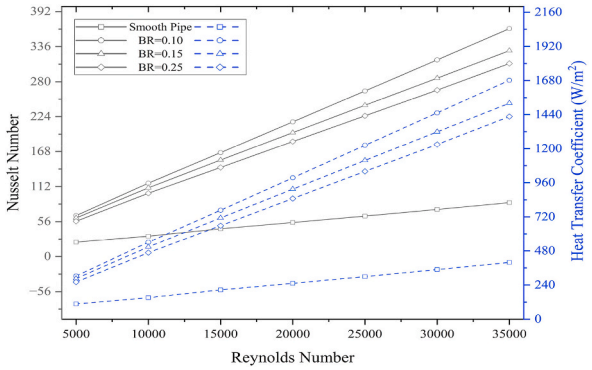

Fig. 6. *Nu* and HTC variation with Re for different blockage ratio.

A modified Brinkman equation was developed to determine the VF of both nanoparticles in the base fluid for hybrid nanofluids [75]:

$$\mu_{hnf} = \frac{\mu_{bf}}{(1-\varphi_{s,1})^{2.5}(1-\varphi_{s,2})^{2.5}} \tag{40}$$

A revised version of Maxwell's theory called the Hamilton and Crosser model [76] has been utilized;

$$k_{nf} = k_{bf}\frac{k_s + (n-1)k_{bf} - \varphi(n-1)(k_{bf}-k_s)}{k_s + (n-1)k_{bf} + \varphi(k_{bf}-k_s)} \tag{41}$$

The thermal conductivity of a hybrid nanofluid is determined using the Maxwell model, which provides a comprehensive equation for estimating the thermal conductivity of a mixture consisting of dispersed solid particles and a base fluid. Therefore, the Maxwell equation's result, Eqn. (42), can be utilized to define:

$$\frac{k_{\mathrm{hnf}}}{k_{\mathrm{bf}}} = \frac{\frac{\left(\varphi_{Al_2O_3}k_{Al_2O_3}+\varphi_{Cu}k_{Cu}\right)}{\varphi} + 2k_{\mathrm{bf}} + 2\left(\varphi_{Al_2O_3}k_{Al_2O_3}+\varphi_{Cu}k_{Cu}\right) - 2\varphi k_{\mathrm{bf}}}{\frac{\left(\varphi_{Al_2O_3}k_{Al_2O_3}+\varphi_{Cu}k_{Cu}\right)}{\varphi} + 2k_{\mathrm{bf}} - \left(\varphi_{Al_2O_3}k_{Al_2O_3}+\varphi_{Cu}k_{Cu}\right) + \varphi k_{\mathrm{bf}}} \tag{42}$$

Thermophysical characteristics of several water-based nanofluids as well as hybrid nanofluids are needed for the current investigation. Basic characteristics of base fluid and nanofluid are presented in Table 7. Moreover, the characteristics of hybrid and water-based nanofluids are shown in Table 8.

4. Code validation

Code validation is an essential requirement to have a firm grasp of the potential and constraints of any numerical activity. Reduced error values can lead to higher precision and better preparation for numerical simulations. The validation was carried out for both corrugated pipe with baffles and smooth pipe. Fig. 4 shows both models having a satisfactory match with the correlations. Fig. 4(a) represents the accuracy of the model with respect to the correlation stated by Hausen [78] and Gnielinsky [79]. The Hausen equation is among the earliest ones that describes how the Nusselt number for a channel with a diameter of D_h varies over the entrance length. This correlation has a limit of $0.6 \leq \mathrm{Pr} \leq 1000$ and $2300 \leq \mathrm{Re} \leq 10^5$. The correlation is expressed as Eqn. (43). From 0.6 to 1000, a wide range of Prandtl numbers are covered by the Hausen equation. Furthermore, Gnielinsky improved this equation. Fully turbulent flows with Reynolds numbers more than 3000 can be analyzed using Eqn. (44).

$$\mathrm{Nu} = 0.037\left(\mathrm{Re}^{0.75} - 180\right)\mathrm{Pr}^{0.42}\left[1 + \left(\frac{2h}{x_1}\right)^{2/3}\right] \tag{43}$$

$$\mathrm{Nu} = 0.012\left(\mathrm{Re}^{0.87} - 180\right)\mathrm{Pr}^{0.4}\left[1 + \left(\frac{2h}{x_1}\right)^{2/3}\right] \tag{44}$$

Where h = channel half-width and x_1 = entry length.

The curved corrugated pipe with an entry region had shown a satisfactory result. Furthermore, the smooth pipe gives a good match for the friction factor correlation given by Petukhov and Blasius in Fig. 4(b). The Blasius equation from White [80] for a single-phase fluid is represented as Eqn. (45). Petukhov and Popov equation [81] is also expressed as Eqn. (46).

$$f = 0.3164Re^{-0.25} \tag{45}$$

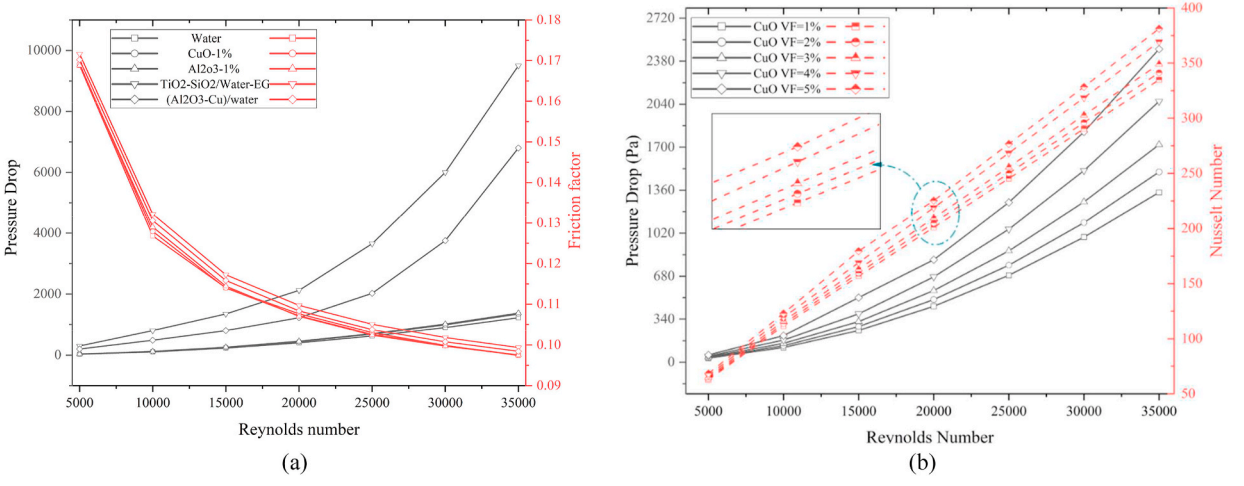

Fig. 7. ΔP and f variation with Re for (a) different nanofluid and hybrid nanofluid (b) utilizing 1%–5% volume concentration of CuO.

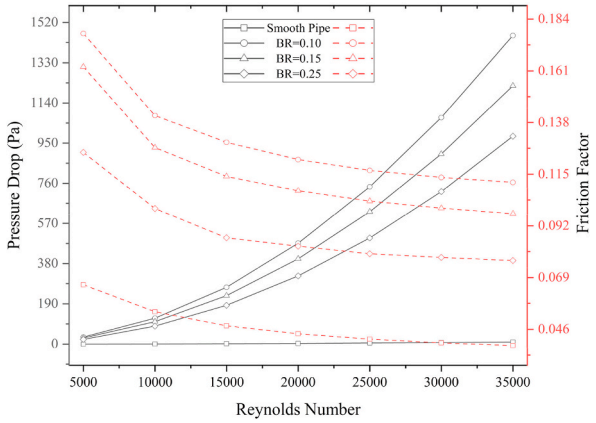

Fig. 8. ΔP and f variation with Re for different blockage ratio.

Table 10
Pressure Drop difference for different models at lower and higher Re

Reynolds Number	Smooth Pipe	BR = 0.25	BR = 0.15	BR = 0.10
5000	0.31527	22.88218	29.17271	33.52846
35,000	10.20869	982.52282	1221.3446	1458.5038

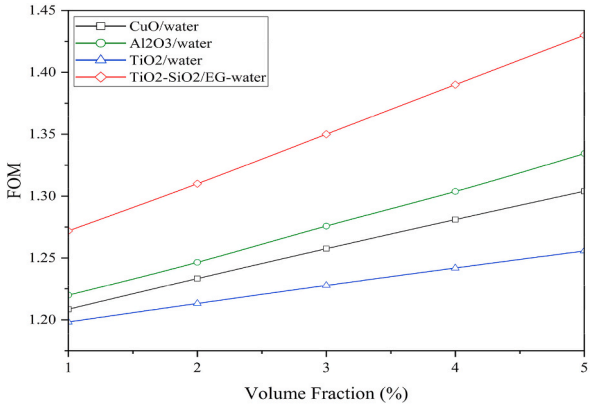

Fig. 9. FOM variation for different VF with Re of 25000 using curved corrugated channel with BR = 0.15 E-shaped baffles.

$$f = (0.790\text{InRe} - 1.64)^{-2} \tag{46}$$

The difference between the relevant correlation and the current work is shown in Table 9. The table shows that there is a significant correlation between the findings and the values of the parameters that are being studied, with a variance of less than 7%. This gives a quite adequate result for further continue the study. Upon numerical examination, it can be observed that the computational findings exhibit a decent level of agreement with both the *Nu* and the friction factor. The present computational model accurately predicts the flow and thermal characteristics of the channel.

5. Results and discussion

To predict the behavior of a curved corrugated channel with baffles, the present numerical simulations, which have been developed specifically for the use of water-based nanofluids, include a broad range of Reynolds Number values (from 5000 to 35000). The first section presents the research of the channel using several kinds of nanofluid and hybrid nanofluid. Afterwards, the design parameter was changed in order to determine which model would work best for the channel.

5.1. Heat transfer (HT) performance

The HT rate by conduction, convection, and radiation is denoted by HTC, which quantifies the thermal conductivity between a solid

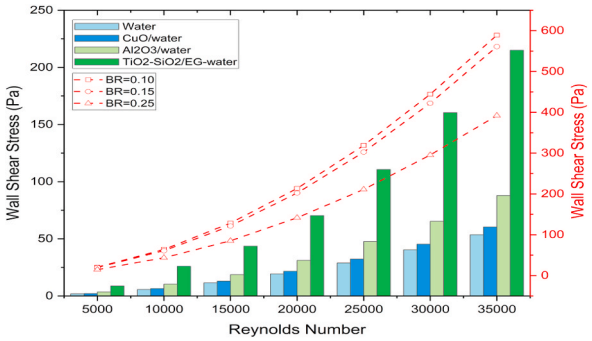

Fig. 10. Wall shear stress distribution for different nanofluid and blockage ratio.

surface and a fluid medium. Fig. 5(a) represents the deviation of both *Nu* and HTC in arrange of 5000≤Re ≤ 35000 for different nanofluid and hybrid nanofluid. Inspecting the figure reveals that increasing the Reynolds number causes both *Nu* number and HTC to increase linearly. The highest HTC was possessed by 2%(Al_2O_3–Cu)/98% Water hybrid nanofluid while the lowest was by SiO_2/Water having a value of 408.32 W/m^2K and 287.78 W/m^2K respectively at a Re of 5000. Because of the improved thermophysical characteristics, which cause the value of (T_w-T_b) to drop, the thermal conductivity, k, has been shown to be considerable important in comprehending the factors contributing to the augmentation of heat transfer. In case of *Nu* number, a different scenario has been observed. The SiO_2 remains the lowest in term of *Nu* number but the highest position was taken by (20% TiO_2-80% SiO_2)/(60% Water-40% EG) hybrid nanofluid having a magnitude of 538.09105 at Re = 35,000. This phenomenon occurs due to a very low magnitude in thermal conductivity and C_P. In the case of single nanofluid, Al_2O_3/water hold the highest position. A little amount of nanoparticles added to a hybrid nanofluid can significantly enhance its thermophysical characteristics. Afterwards, the hybrid nanofluid's *Nu* and HTC values are much greater than those of a single nanofluid, especially at higher Re.

Fig. 5(b) shows the variation of utilizing different volume fractions of a nanofluid. A range of 1%≤φ ≤ 5% has been set to find the optimum value. A similar trend can be observed where increasing Re, increases the *Nu* and HTC in correlation with the increment of the nanofluid's φ. The higher the VF, the greater heat transfer. Using a VF of 5% can cause HTC to increase by 18.41% compared to 1%. The Optimum *Nu* number is obtained with 5% VF for Al_2O_3/water having a value of 366.83 at Re = 35,000.

The design of the model has a great impact on the thermophysical properties of the channel. Fig. 6 illustrates the deviation of *Nu* and HTC due to the change in the blockage ratio. For a smooth channel, the HTC holds a very small magnitude compared to the modified models. Decreasing the blockage ratio can cause the properties to increase. At a BR = 0.10, the highest HTC can be observed. For a BR of 0.10, 0.15 and 0.25, the *Nu* number values are 65.71, 61.90 and 56.56 respectively for Re = 5000. Decreasing the blockage ratio causes a restriction in fluid to pass the baffles which leads to turbulence in the fluid flow. This increases the friction along with the E shaped baffle. Consequently, the HTC increases causing to transfer more heat.

5.2. *Pressure drop characteristics*

The investigation focuses on the evaluation of nanofluid performance, specifically in relation to pressure drop, which is influenced by changes in shape. The incorporation of nanoparticles into nanofluids results in an increase in both density and viscosity, hence requiring a significant amount of pumping power to effectively manage fluids with high density. Fig. 7(a) represents the variation of pressure drop and friction factor for different nanofluid and hybrid nanofluid flown in a curved corrugated pipe with E shaped baffles. A high deviation of pressure drop can be visualized for the hybrid nanofluid compared to single nanofluid. (20% TiO_2-80% SiO_2)/(60% Water- 40% EG) has the lead in pressure drop continued by Al_2O_3–Cu/water. Increased viscosity, interactions between nanoparticles, and modifications to flow patterns can all contribute to a greater pressure drop in hybrid nanofluids. Sententiously, TiO_2–SiO_2/Water-EG nanofluid has the highest friction factor. Increasing the Re number, makes the pressure drop rise while decreasing the friction factor. Pressure drop increases as the Re rises and the flow becomes turbulent because of increased mixing and energy dissipation.

Using hybrid nanofluid can increase the ΔP over single nanofluid. Within laminar flow, it is frequently noted that the friction factor is higher, leading to a higher energy dissipation that can be caused by viscous processes. Because turbulent flow is more energetic and the fluid mixes more effectively, resulting in less viscous dissipation, the friction factor can be lowered. TiO_2–SiO_2/Water- EG has a friction factor of 0.17021 at Re = 5000 which turns to 0.09842 when Re is increased to 35,000.

Fig. 7(b) shows the deviation of pressure drop and Nusselt number for CuO/water nanofluid for a volume fraction range of 1%≤φ ≤ 5%. Both *Nu* and ΔP increases while raising the Re equivalently the VF. CuO/water of 5% VF has the highest pressure drop and Nusselt number. An increment of 84.440% can be observed by using 5% VF over 1%. Similar phenomena are happening in all the existing single nanofluid and hybrid nanofluid.

Change in shape can cause the pressure drop and *f* to be influenced. Corrugated sections and baffles create turbulence and fluctuations in the velocity profile, which causes a larger pressure loss in the corrugated channel than in the smooth one. The existence of corrugations inside channel leads to an increase in the total surface area, which raises frictional losses and further reduces pressure. The impact of the boundary layer disruption generated by the baffles and corrugations is more noticeable at low Re because the

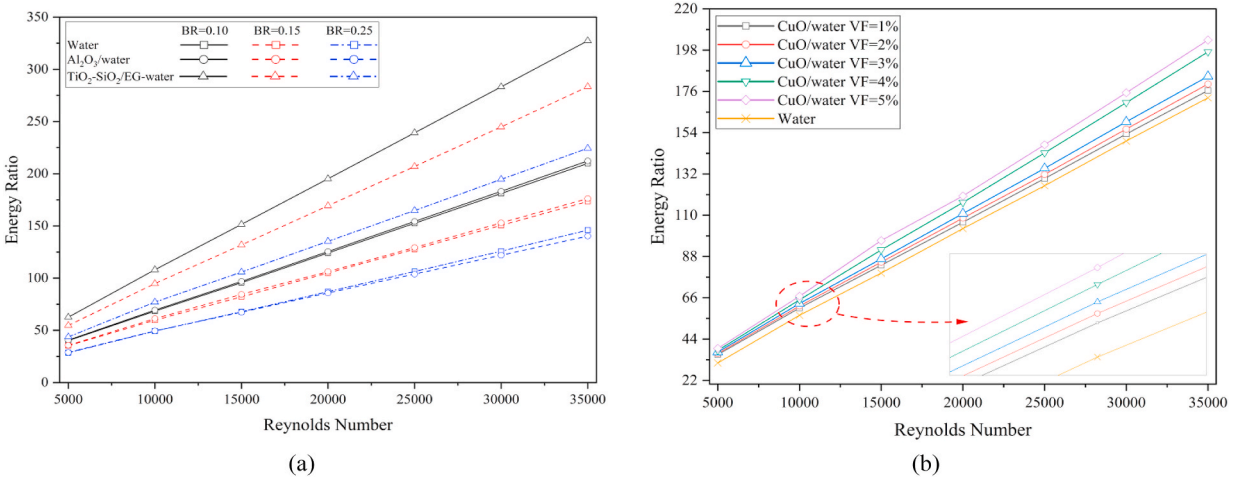

Fig. 11. Variation of energy ratio for (a) different blockage ratio (b) different VF of CuO/water nanofluid.

Table 11
Energy ratio for different BR.

Blockage ratio	Nanofluid	Energy ratio
BR = 0.25	TiO_2–SiO_2/EG-water	164.781
	Al_2O_3/water	103.913
BR = 0.15	TiO_2–SiO_2/EG-water	206.947
	Al_2O_3/water	129.354
BR = 0.10	TiO_2–SiO_2/EG-water	239.195
	Al_2O_3/water	154.336

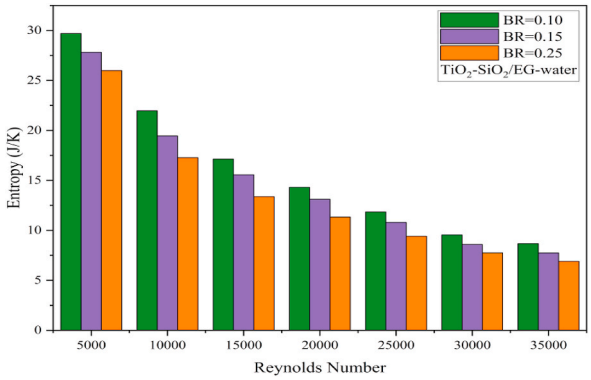

Fig. 12. Entropy generation for curved corrugated channel with different BR.

thermal boundary layer is significantly broader and the flow's turbulence strength is lower. Fig. 8 represents the change in ΔP and *f* for a smooth pipe and different blockage ratio using Al_2O_3/water. Smooth pipe has both the lowest value whilst a BR of 0.10 can create the highest pressure drop and friction factor. When the blockage ratio is decreased to 0.10 from 0.25, the fluid has less space to flow through the baffle. This causes a turbulence in the lower region and a vortex is being created. This increment in surface area is the primary reason of this enhancement. At a Re of 25,000, the ΔP is 982.52 Pa using a blockage ratio of 0.25, 1221.34 Pa using BR = 0.15 and 1458.50 Pa using BR = 0.10 which is the highest. At lower Re, the pressure drops don't have a great deviation. Increasing Re, causes the deviation to increase as shown in Table 10.

5.3. Mouromtseff number

A useful metric for assessing the heat transfer efficiency of different fluids is the dimensionless Mouromtseff number (MO). Greater Mo number values are indicative of enhanced appropriateness for thermal applications as they facilitate the assessment of fluid heat transfer efficiency. The determination of the MO number for the fully developed internal flow is established by Yu et al. [82];

$$Mo = \frac{\rho^a . k^b . C_p^c}{\mu^d} \tag{47}$$

Applying the Dittus-Boelter equation for conventional fluids, as described by Pak et al. [70], yields the parameters. For the turbulent flow inside the body, as per Vajiha and Das [83], Mouromtseff number ratio (*FOM*) can be written as;

$$FOM = \frac{Mo_{nf}}{Mo_{bf}} = \frac{h_{nf}}{h_{bf}} = \frac{\rho_{nf}^{0.8} . C_{pnf}^{0.5} . k_{nf}^{0.5}}{\mu_{nf}^{0.3}} . \frac{\mu^{0.4}}{\rho^{0.8} . C_p^{0.4} . k^{0.6}} \tag{48}$$

In terms of Mouromtseff number ratio, Fig. 9 demonstrates the performance of four types of nanofluid in comparison to water, a standard heat transfer fluid. A greater FOM value has been obtained by increasing the VF(φ) of nanofluid. FOM has been always obtained higher than 1 for every nanofluid ranging from $1\% \leq \varphi \leq 5\%$. The highest magnitude is shown by TiO_2–SiO_2/EG-water where the FOM is 1.27 and 1.43 for 1% and 5% respectively. The lowest value is observed from TiO_2/water. The most favorable result is acquired by 5% TiO_2–SiO_2/EG-water hybrid nanofluid.

5.4. Wall shear stress characteristics

A rise in pressure drop is attributed to the increasing viscosity of nanofluids with concentration. As demonstrated by Fig. 10, an increase in wall shear stress results from a rise in fluid viscosity. Higher pressure drops are the result of increasing shear stress on the wall. Re increases lower the temperature and velocity boundary layer thickness, which lessens the resistive effect of the nanofluid as it

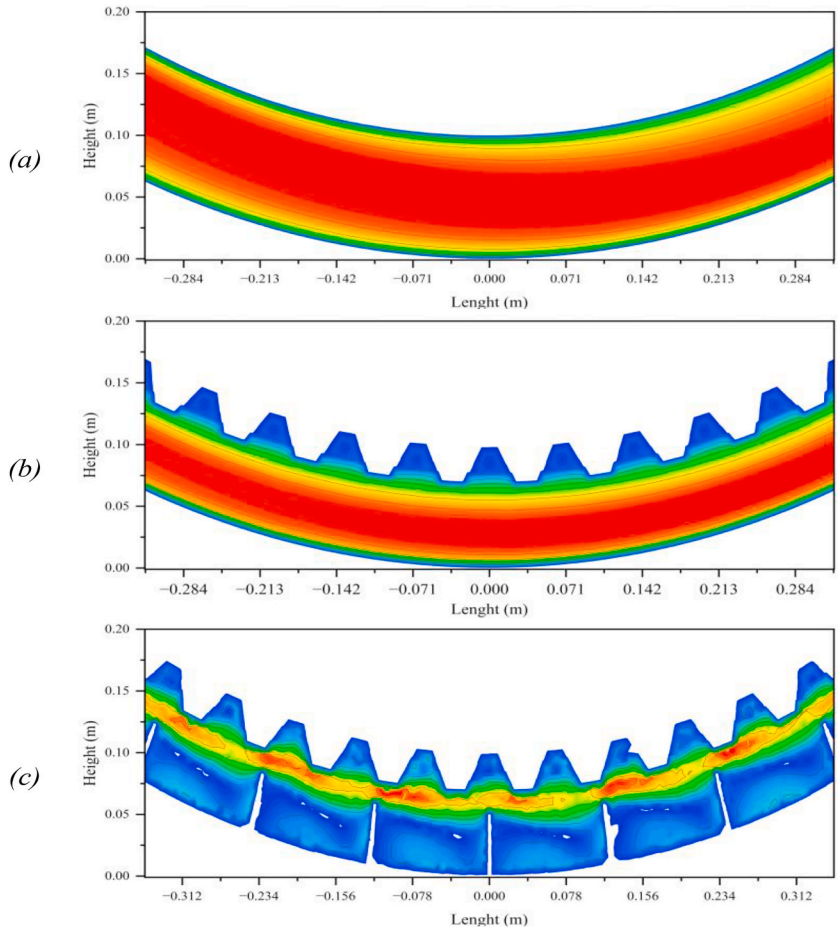

Fig. 13. Velocity contours at Re = 15,000 for the following channels: (a) smooth; (b) corrugated without baffles; and (c) corrugated with baffles.

flows through the channel. A rise in the concentration of nanoparticles might alter the density and viscosity of the nanofluid. A higher viscosity might change the flow characteristics close to the wall, which would affect the shear force acting on the wall. Nanofluids typically transmit heat more efficiently than their basic fluid counterparts. A fluid's viscosity and turbulence characteristics may be impacted by changing temperature gradients near the wall as a result of increased thermal conductivity. Consequently, the wall shear stress will be impacted. As Reynolds number increases the wall shear stress also increases. This phenomenon is due to the increased pressure drop. Using TiO_2–SiO_2/EG-water hybrid nanofluid can cause greater wall shear stress. Water has the lowest stress followed by CuO/water. The blockage ratio also varies the wall shear stress. A blockage ratio of 0.10 can obtain the highest magnitude due to vortex generation and well mixing of fluid. For BR = 0.25, 0.15 and 0.10 the stresses are 211.14 Pa, 302.67 Pa and 319.03 Pa respectively for a Re = 25,000. Furthermore, using the same blockage ratio of 0.15, TiO_2–SiO_2/EG-water, Al_2O_3/water and CuO/water has a magnitude of 110.67 Pa, 47.61 Pa and 32.34 Pa respectively. The highest wall shear stress can be obtained by using hybrid nanofluid along with a blockage ratio of 0.10.

5.5. Energy ratio

The ratio of the Nusselt number to the Euler number is commonly known as the energy ratio (ER). This concept could be implemented to investigate nanofluids and assess their thermodynamic properties. The energy ratio may be written as.

$$ER = \frac{Nu}{Eu} = \frac{d}{4L}.Re \tag{49}$$

Eqn. (27) is used to get the *Nu* and ΔP/unit length of the channel is used to calculate the Euler number. Fig. 11(a) demonstrates the deviation of ER for water and 2 types of nanofluid consisting of one nanofluid along with the blockage ratio. The maximum ER was obtained using BR = 0.10 with TiO_2–SiO_2/EG-water hybrid nanofluid. The top three lines in Fig. 11(a) indicates the influence of hybrid nanofluid. A linear increment in ER has been observed while increasing the Reynolds number. Water has the lowest ER for all three blockage ratios. Fig. 11(b) depicts the influence of volume fraction in ER. Increasing the volume fraction can cause the energy ratio to get higher while Re also increases. Similar characteristics exist in all types of nanofluid, as shown in Table 11.

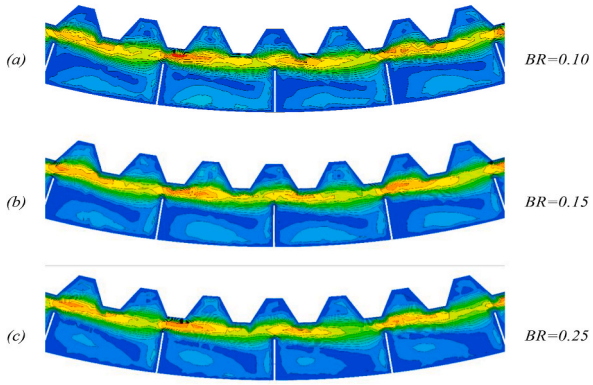

Fig. 14. Observing the velocity profile contour at various BR values.

5.6. Entropy generation

An effective method for assessing and enhancing heat exchangers' thermal performance is the study of entropy generation. Entropy generation indicates a system's irreversibility, and reducing it leads to more efficient systems. The formula for computing volumetric entropy generation is provided.

$$\Delta S \equiv \int_{rev} \frac{\delta Q}{T} \tag{50}$$

The entropy, assuming a compressible fluid, may be written as follows:

$$\Delta S = C_p \, ln\left(\frac{T}{T_{ref}}\right) - Rln\left(\frac{P}{P_{ref}}\right) \tag{51}$$

Fig. 12 represents the entropy generation for different blockage ratio of the curved corrugated channel. Because of increased mixing, turbulence creation and viscous dissipation can both lead to higher entropy generation. TiO_2–SiO_2/Water-EG is used for a Reynolds number range of $5 \times 10^3 \leq Re \leq 35 \times 10^3$. It can be observed that the entropy generation reduces as the Re increases. For a BR = 0.10 the highest entropy generation can be seen due to higher obstacles whilst the lowest entropy generation occurs at BR = 0.25. Maximum entropy of 29.70J/K was found at BR = 0.10 and minimum entropy of 6.89J/K at BR = 0.25.

5.7. Flow behavior investigations

5.7.1. Velocity profile

As seen in Fig. 13, the primary flow path of the channel can be altered by the presence of corrugation and baffles, permitting secondary flow swirls, which are thought to be a major cause of improved heat transfer. Velocity contours illustrate how the presence of corrugation and baffles affects the velocity along the channel walls. While secondary flow is evident in Fig. 13(b) and (c), also concentrated after and before the baffles and corrugation, it is absent from the smooth channel in Fig. 13(a). Since corrugations and baffles have considerable effects, the corrugated channel with baffles offers greater mixing. Compared to a channel without baffles, the channel having baffles has superior mixing flow pattern because of velocity magnitude is noticeably higher. Two additional recirculation regions are generated near the upper wall and along with the baffles of the curved-corrugated channel as a result of the baffle pressing down on the irregularly formed recirculation zone.

Blockage ratio can greatly impact the flow of the fluid. A smaller blockage ratio means small region to pass the baffles. Fig. 14 represents the different velocity profile for BR = 0.10, 0.15, and 0.25. It can be observed that the fluid flow has been changed due to the design change. Due to the baffles a vortex region is being created in the lower part of the channel which causes a negative velocity. This negative velocity can heavily effect in the heat transfer enhancement due to higher mixing. The vortex region is being affected by baffles. In order to understand the velocity through the baffles, Fig. 15 is illustrated. The transverse plane of the channel has been taken into consideration.

From close observation, the flow phenomena can be understood in Fig. 15. On the left side the velocity can observed, right above the baffles the velocity decreases when BR is taken from 0.10 to 0.25. But the velocity through the baffles increases because the area of open space in baffles increases allowing more fluid to pass it. A three-dimensional flow characteristic has been used to visually represents how much fluid can pass through the baffles. When BR = 0.10, less fluid can pass through the baffles which cause more fluid to be flown over the baffles. This causes a highly red zone over the baffles. A boundary layer formation can also be seen around the 2 gaps of the baffles. High fluid can pass through the gap when BR = 0.25 which causes less fluid to flow over the baffles.

Fig. 16 shows the vector velocity of the channel. The velocity increases in the lower part of the channel when the gap is larger. A better visualization of the vortex creation can be seen where the vector direction gets altered from the fluid flown direction. This phenomenon occurs in both the corrugation area and before and after the baffles. This vortex causes a negative velocity to be generated

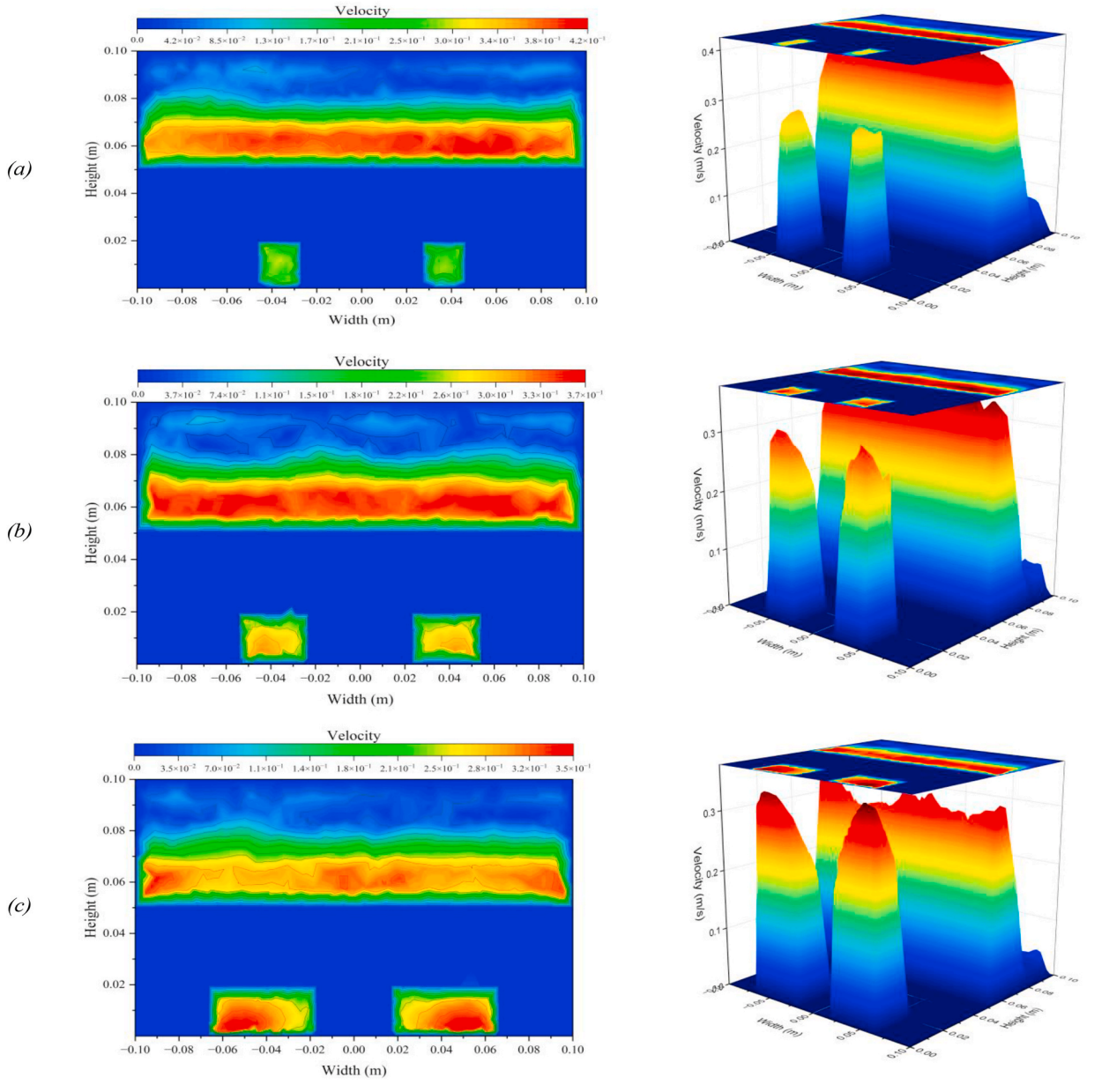

Fig. 15. Different blockage ratios' velocity profiles in the transverse planes of curved-corrugated channels: (a) BR = 0.10, (b) BR = 0.15, and (c) BR = 0.25.

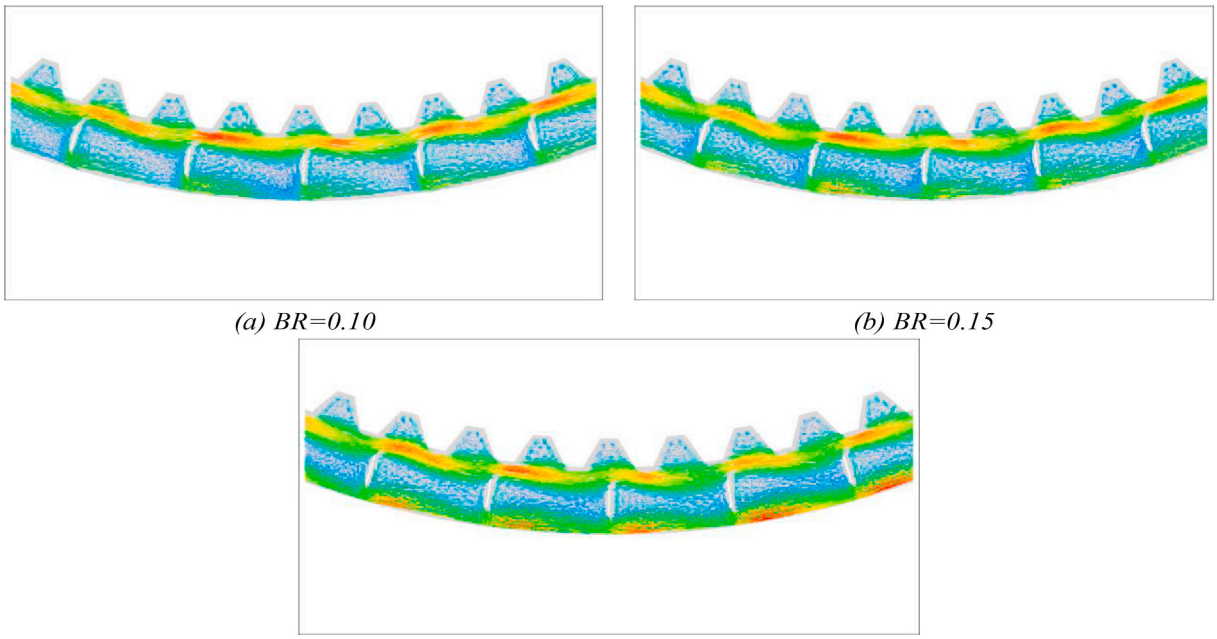

Fig. 16. Observing the velocity vector at various BR values.

which is shown in Fig. 16(b) for a BR = 0.15 using Al_2O_3/water nanofluid.

Various line sections have been taken over the channel to understand the velocity profile along time pipe. The profile shows a negative velocity has been generated at a height of 0.04 mm due to the presence of the baffles and another negative region from 0.085 to the top surface of the channel due to the presence of corrugation shown in Fig. 17. 2 lines have been placed on the inlet region and outlet region which shows a traditional boundary layer formation due to the no slip condition. At the end of the channel the boundary layer was fully developed. One specific line was taken at the middle of the pipe where a linear zero velocity can be seen created due to the baffles.

Fig. 18 depicts the streamline, offering insights into the fluid flow within the channel walls and enhancing our understanding of the flow dynamics and heat transfer characteristics. The geometric arrangements of the flow exhibit a significant influence on the generation of vorticity inside fluid flow. The generated vortices offer a notable advantage in terms of augmenting heat transfer by promoting fluid mixing within the channel.

5.7.2. Temperature profile

Due to recirculation or secondary flow regions, the temperature differential is notable near corrugations and baffles. Fig. 19(c) performs more effectively than Fig. 19(b) since it has both corrugations and baffles, nevertheless Fig. 19(a) lacks both. According to this, it is evident that in scenario (c), The approach of combining warm fluid in close proximity to the corrugated wall with cold fluid positioned in the center area of the channel or at the bottom wall is very praiseworthy. A better mechanism for convection heat transfer is to increase flow mixing and decrease boundary layer thickness. Since a constant heat flux of 1000 W/m^2 is used on the upper surface of the channel, a smooth line of the temperature profile. A further study was taken into consideration in Fig. 20 where the temperature profile is created using different lines mentioned in Fig. 17. It can be observed in the plots that the temperature rises at the top of the channel near the top surface. Due to an increment in velocity the temperature can be higher. At line 11, situated right before the outlet, the temperature remains constant from lower to upper surface due to no heat flux present there.

5.7.3. Turbulent kinetic energy

Turbulent kinetic energy (TKE) quantifies the magnitude of energy related to the stochastic variations in velocity inside a turbulent fluid motion. The presence of corrugations and baffles had an impact on the amount of turbulence, as can be inferred from Fig. 21 by observing the turbulent kinetic energy contours, with the greatest rates happening both before and after the baffles and near the corrugations of the surface. The distribution of turbulent kinetic energy exhibits variation between the upper and lower walls of the channel, which can be attributed to the lack of corrugations on the bottom wall. Consequently, it may be concluded that baffles and corrugations greatly enhance thermal performance. Concurrently, the pressure differential will escalate due to heightened interaction between the amalgamating fluid and the boundaries of the channel.

As the blockage ratio (BR) increases, indicating a reduction in the width of the gaps in the baffles (BR = 0.10) shown in Fig. 22(a). More flow disruption can result from smaller spaces between baffles, which increases turbulent kinetic energy and turbulence. This phenomenon occurs due to the increased presence of barriers in the flow, resulting in fluctuations in velocity and dissipation of energy.

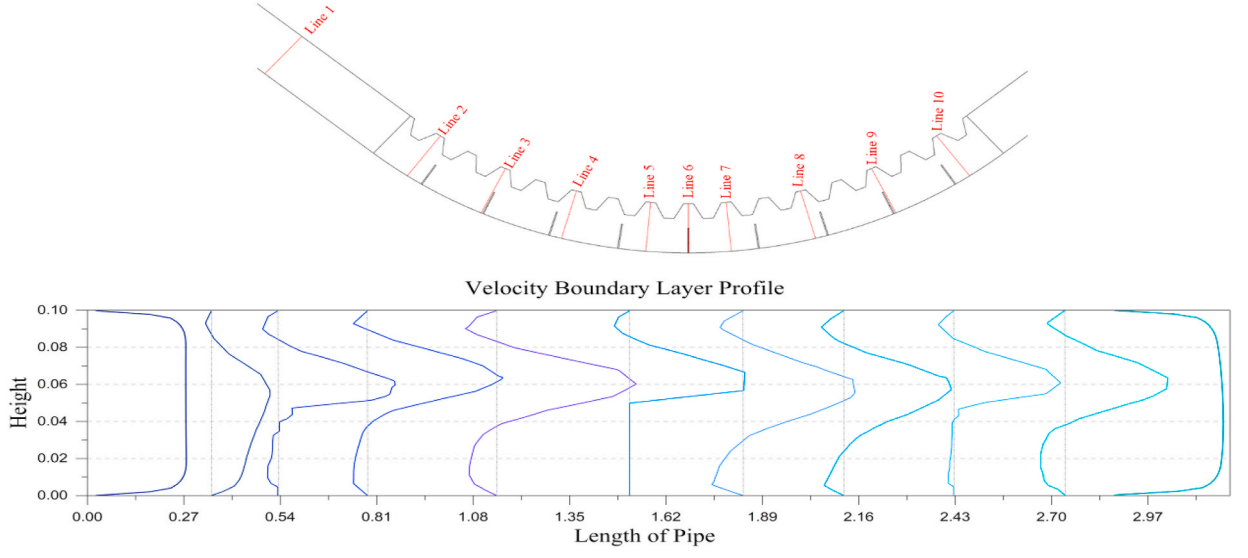

Fig. 17. Velocity boundary layer profile at different line section of the channel.

Fig. 18. Observing the velocity streamline at various BR values.

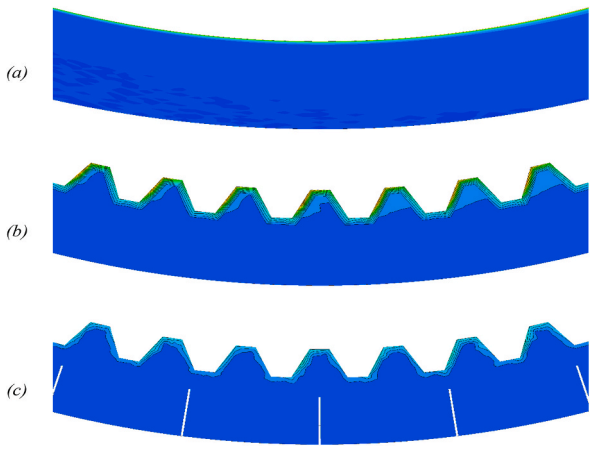

Fig. 19. Temperature Contours at Re = 15,000 for the following channels: (a) smooth; (b) corrugated without baffles; and (c) corrugated with baffles.

Better mixing of the fluid within the channel may be encouraged by the increased turbulence. In order to facilitate the exchange of momentum and promote the generation of larger TKE, the fluid flow must effectively overcome the restriction posed by the baffles, hence enabling the interaction of multiple fluid layers. The dissipation rate of energy in the flow will be augmented as a result of the heightened turbulence, resulting in elevated levels of TKE. The TKE may decrease slightly in scenarios with broader gaps (BR = 0.15), as broader gaps create more structured flow patterns shown in Fig. 22(b). Although baffles still cause turbulence, the intensity may be reduced compared to BR = 0.10, indicating that broader gaps may facilitate more structured flow patterns. The TKE values may exhibit a decrease in comparison to both BR = 0.10 and BR = 0.15. The presence of wider gaps may potentially result in less obstructions, hence facilitating more seamless and steady flow patterns.

Right side of Fig. 22 depicts the variation of turbulent intensity for different BR using Al_2O_3/water nanofluid at Re = 15,000. A narrower blockage ratio (BR = 0.10) in a baffle leads to a more complex flow path, causing higher velocity fluctuations and increased turbulent intensity. This can result in rapid changes in velocity, increasing the intensity of these fluctuations. Different blockage ratios can result in varying levels of intensity at different channels. Narrower gaps may create pockets of high turbulence and intensity behind baffles, while wider gaps allow for a more regular flow structure, reducing velocity fluctuations and intensity. Larger gaps allow for more ordered and less turbulent flow, resulting in reduced fluctuations and intensity. With a close observation, there is a high turbulent intensity zone right at the left upper corner of the baffles. In fluid dynamics, this is frequently observed when flow encounters obstructions that cause the fluid to separate from the surface and produce eddies or recirculation zones. The geometric properties of the baffles and the curvature of the channel cause disruptions to the fluid's velocity profile. It is possible for the previously indicated disturbance to cause changes in the pressure and velocity distribution over the baffles' surface. The fluid may separate from the baffles' surface as a result of the disruption of fluid flow. When the flow undergoes separation, it gives rise to a distinct region where the fluid exhibits a deviation in its direction of motion, typically manifesting as an upstream movement or a whirling pattern. The recirculation zone exhibits an intricate interaction between vortices and eddies, resulting in a notable augmentation of turbulence. As the fluid undergoes various directional movements and internal interactions, the amplitude of velocity fluctuations increases, resulting in elevated levels of turbulent intensity. The amplification of TKE and turbulent intensity can occur due to the swirling and mixing of fluid within the recirculation zone. The flow originating from the main channel interacts with the recirculating fluid in the vicinity immediately above the recirculation zone. The interplay between the contrasting flow directions, along with the velocity gradient existing between these two locations, contributes to heightened levels of turbulence and turbulent intensity.

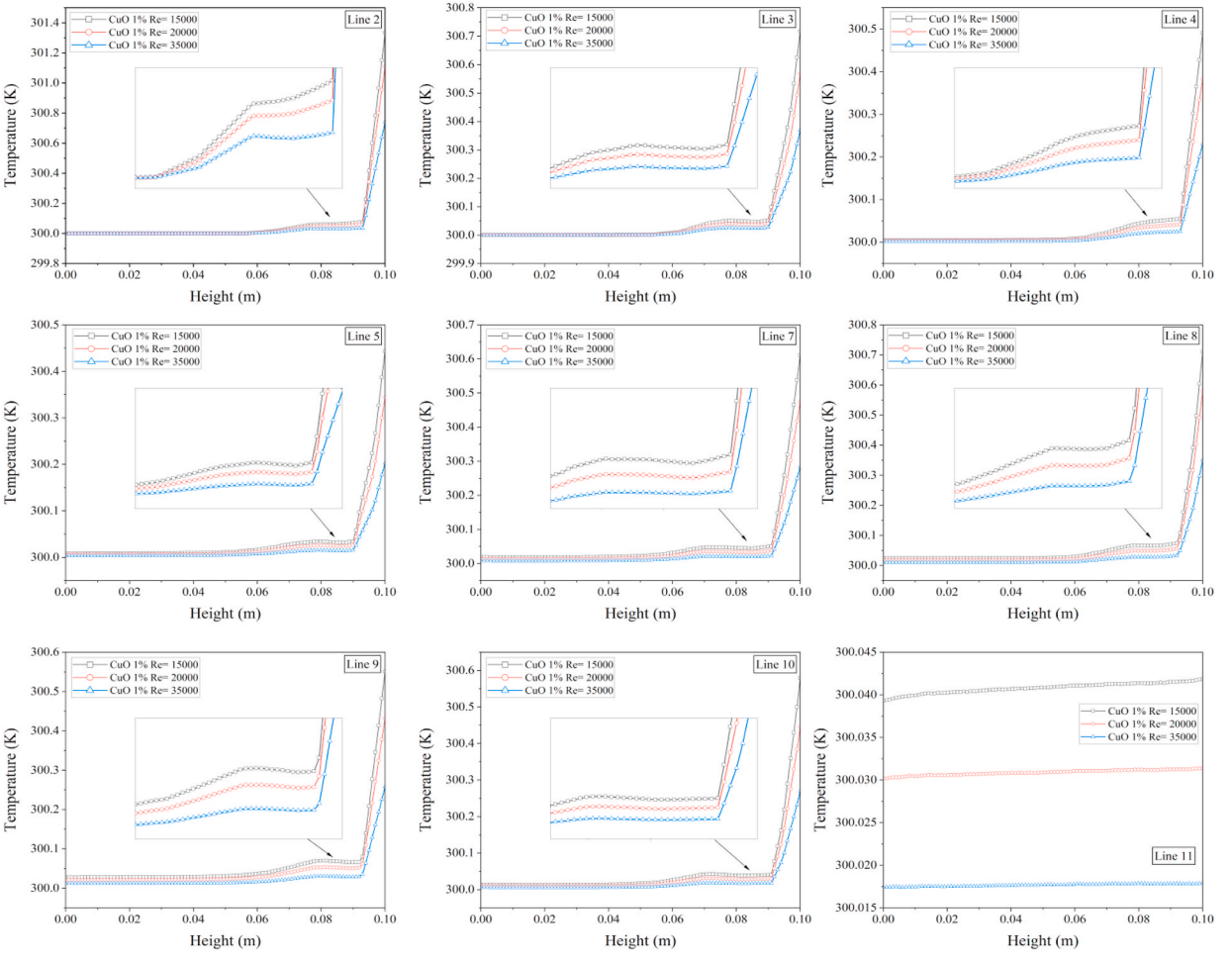

Fig. 20. Temperature profile at different line section of the channel.

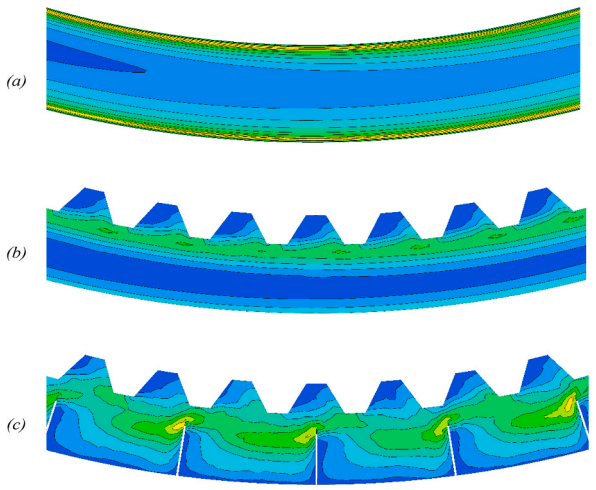

Fig. 21. TKE Contours at Re = 15,000 for the following channels: (a) smooth; (b) corrugated without baffles; and (c) corrugated with baffles.

Fig. 23 illustrates Turbulent kinetic energy contours in transverse planes. It can be observed from the legend that the TKE has been reduced in case of BR = 0.25. The distribution of TKE can be visualized more easily. Increasing the gap causes a larger amount of TKE thought the baffles while lowering above it.

In order to understand the pressure distribution in the fluid flow, different line section has been taken as illustrated in Fig. 24. Using these lines, the exact pressure at that location has been specified in Fig. 17 along the height of the channel. At line 2 the pressure is lower at the upper surface compared to the lower surface where the baffle is situated. Line 3 has been taken right before the baffle, indicating a sudden rise in the pressure due to the fluid not been able to surpass the obstacle. Line 5 and 7 show quite similar characteristics. After line 8, the lower surface starts to feel a lower pressure due to the pressure drop after all the baffles along the length of the channel. Line 11 was taken right before the outlet where the pressure has drastically dropped. A negative pressure can be seen at line 10, at the lower surface of the pipe.

5.7.4. Shear stress observation

The effect of baffles and corrugation can be highly noticed in Fig. 25 for the wall shear stress distribution. In a smooth channel there is a constant shear stress across the channel but a very low stress at the bottom surface. In Fig. 25(b), the stress is very lower due to the presence of corrugation but still a high stress across the mid-section of the pipe. A major change in the contour can be observed in Fig. 25(c) due to the presence of baffles which causes a vortex shedding that reduces the stress. From this point of view, adding baffles and corrugation can increase the vortex shedding resulting in a lower shear stress across the channel.

The distribution of shear stress is greatly influenced by the existence of vortex shedding from the corrugations and baffles placed along the walls of the curved-corrugated channel, as seen on the right side of Fig. 25. The region exhibiting a reduced shear stress for BR = 0.10 is comparatively smaller in size as compared to other scenarios, owing to the deceleration of velocity within the viscous sub-layer at low BR values. The baffle structure is in close proximity to the zones exhibiting elevated shear stress. Following the installation of the baffle, the shear stress along the streamwise direction experiences a decrease and subsequently diminishes due to a reduction in wall limitation. The vortex shedding phenomena intensifies with increasing Reynolds number. Interaction between the top vortices brought on by corrugations and the associated baffle generates this shedding process. As a result, the channel walls are struck by the shedding vortices' increased velocity fluid flow via a viscous sub-layer. The shear stress seen at BR = 0.25 has a larger magnitude compared to earlier instances, suggesting an increase in frictional losses.

5.7.5. Entropy distribution

The entropy generation is affected by the various channel configurations, as seen in Fig. 26. For the smooth channel a constant entropy can be observed at the upper surface of the channel. Adding corrugations creates a drastically change in the entropy generation as seen in Fig. 26(b). Entropy generation is quite low in the middle of the channel and very significant in the corrugated part. Entropy generation in the corrugated channel is distributed uniformly, with a greater value towards the corrugation's edge. When compared to other geometries, the corrugated channel's edges create more turbulence and vorticity, which increases entropy production. Adding the baffles has shown a decrement in the entropy generation. This is because of the secondary flow created by the baffles.

On the right side of Fig. 26, the effect of BR can be demonstrated where the maximum entropy generation takes place when the blockages ratio is 0.10, followed by 0.15 and 0.25. This means that, a turbulent and fluctuating flow can cause the entropy to highly generate. Smaller blockage ratio will cause the flow to move more fluently through the channel and baffles allowing less heat to be generated. A narrow blockage ratio will increase the turbulence and cause more heat generation sententiously more entropy to be generated.

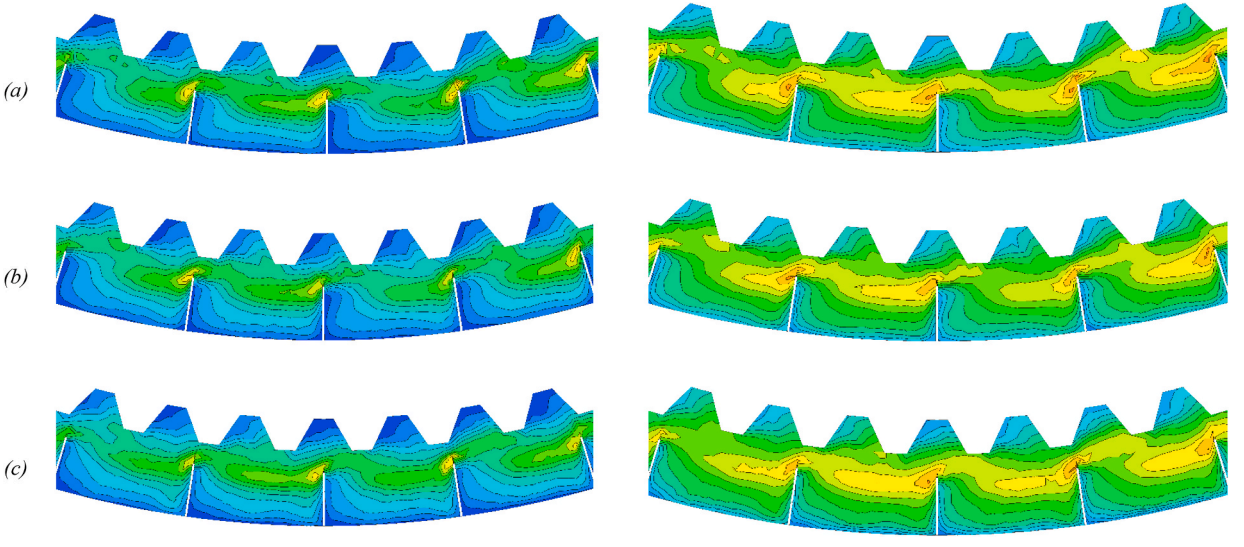

Fig. 22. TKE (left) and Turbulent Intensity (right) Contours of curved-corrugated channel with different blockage ratios, (a) BR = 0.10, (b) BR = 0.15, (c) BR = 0.25.

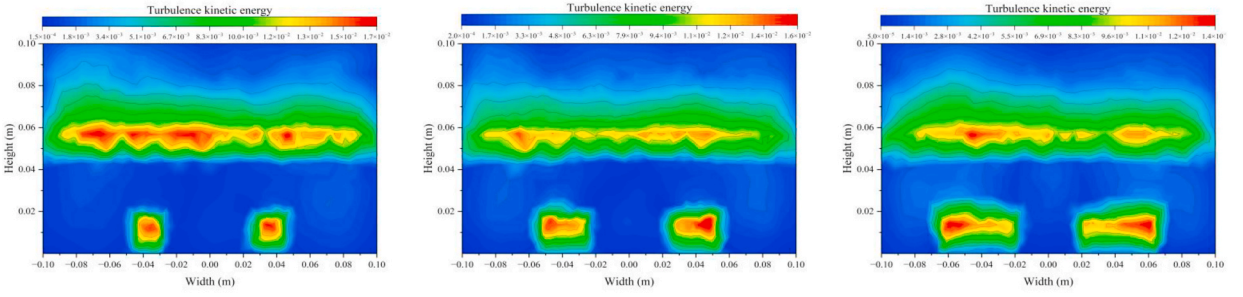

(a) BR=0.10 *(b) BR=0.15* *(c) BR=0.25*

Fig. 23. TKE contours in transverse planes at different blockage ratio.

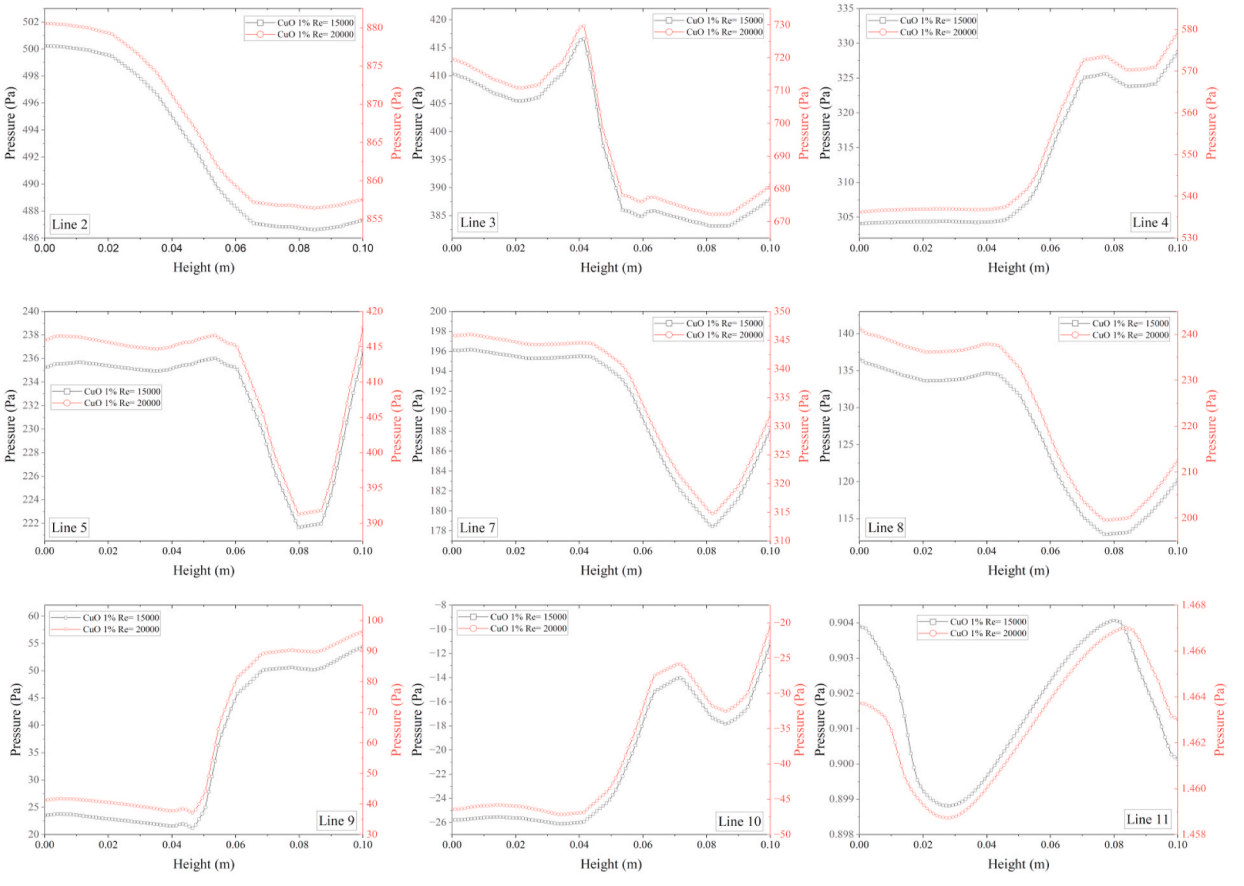

Fig. 24. Pressure profile at different line section of the channel.

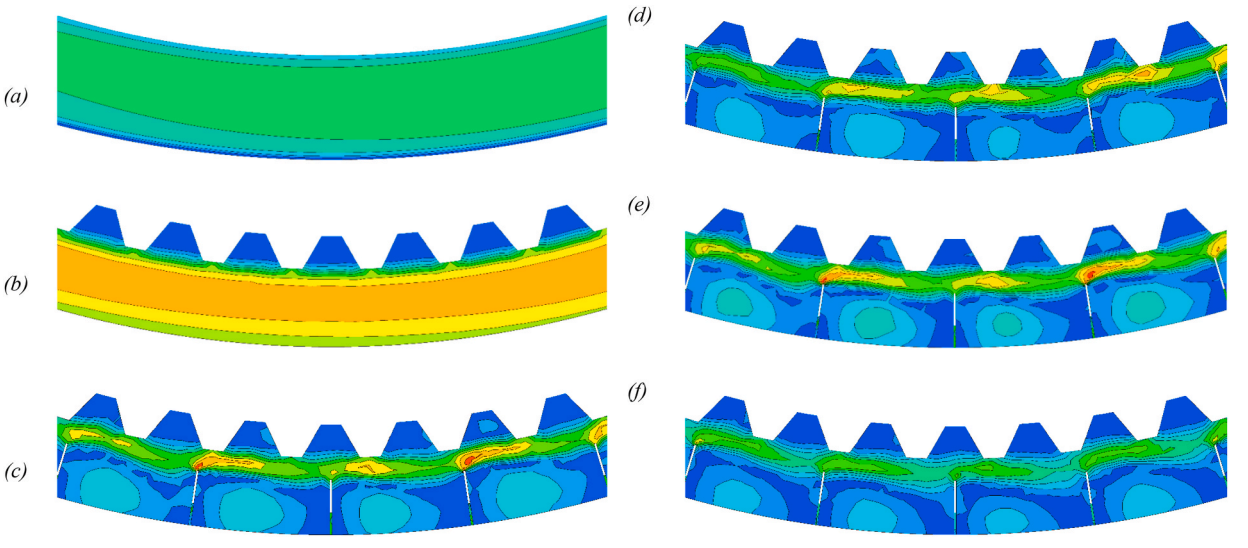

Fig. 25. Shear Stress Contours at Re = 15,000 for the following channels: (a) smooth; (b) corrugated without baffles; and (c) corrugated with baffles, and different blockage ratios, (d) BR = 0.10, (e) BR = 0.15, (f) BR = 0.25.

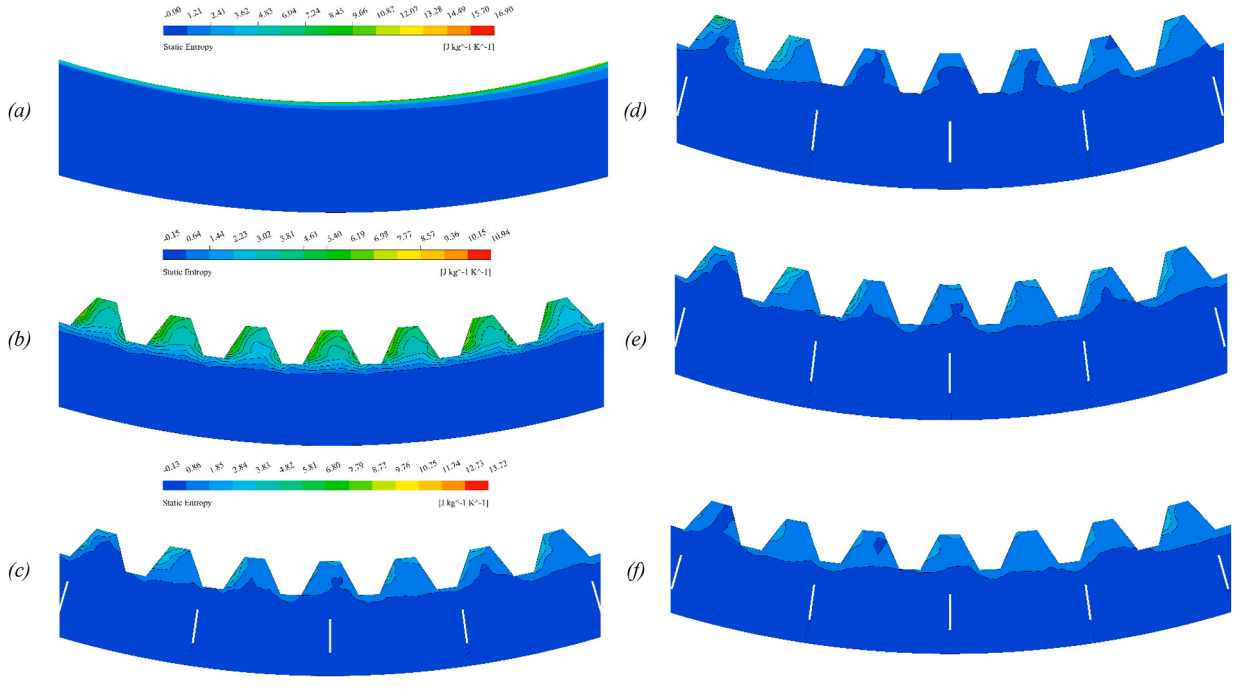

Fig. 26. Entropy distribution Contours at Re = 15,000 for the following channels: (a) smooth; (b) corrugated without baffles; and (c) corrugated with baffles and different blockage ratios, (d) BR = 0.10, (e) BR = 0.15, (f) BR = 0.25.

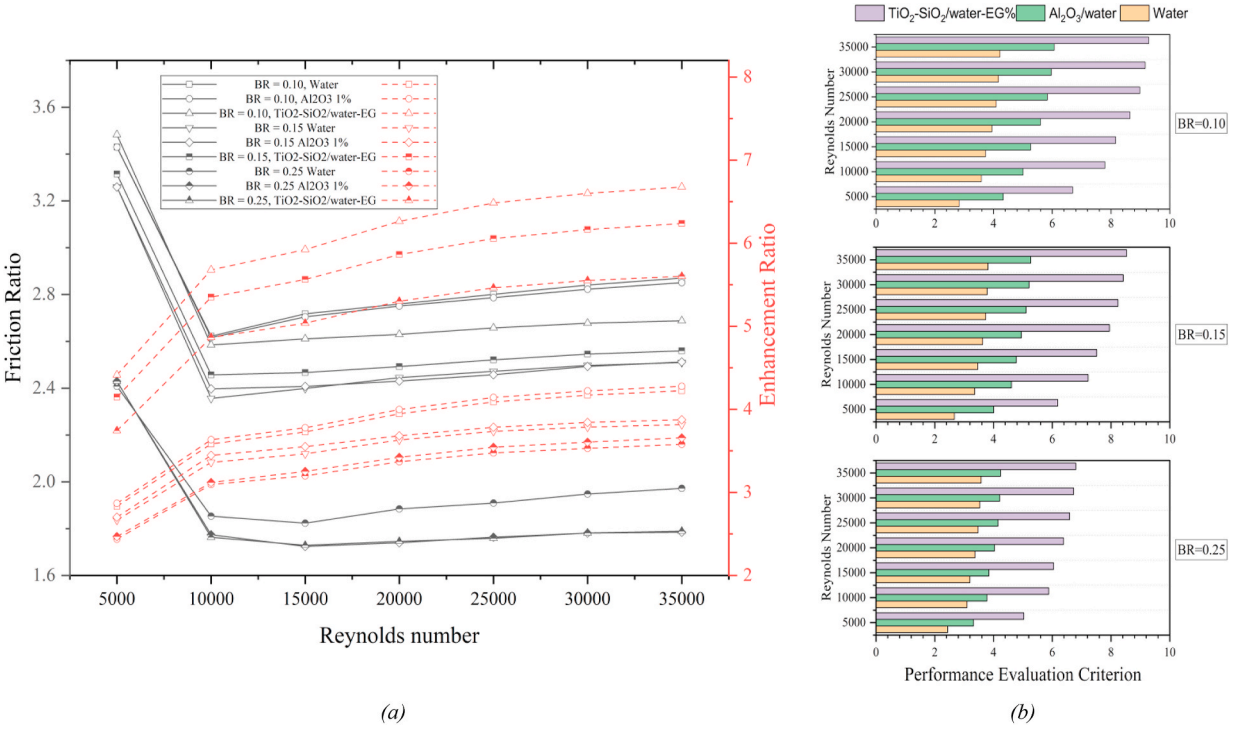

Fig. 27. Effects of varying blockage ratios (BR) on flow performance and heat transfer: (a) Friction ratio and enhancement ratio; (b) PEC.

5.8. 5.8 Performance Evaluation Criterion

The addition of nanofluids to curved corrugated channels can greatly enhance heat transmission, as the previous section described. Allowing the pressure to decrease is usually necessary to improve heat transmission through the use of corrugated channels. A higher PEC ratio results in improved heat transfer performance even with an increase in pressure drop. Additionally, the PEC ratio gives an indication of how well the system's nanofluid is working. Fig. 27 represents the variation of friction ratio, enhancement ratio and PEC for different nanofluid used in three types of blockage ratios. These 3 parameters have been calculated using Eqns. (30)–(32).

Observing Fig. 27(a), the enhancement ratio has increased for a higher Reynolds number while the friction ratio has primarily decreased then has a very small raise. More turbulent flow is frequently the result of a higher Re. Mixing can be improved by turbulence, which can lead to improved heat transmission. Increased Reynolds numbers have the potential to improve heat transfer rates by dispersing the thermal boundary layer close to the surface. This could be particularly pertinent if the flow changes from a laminar to turbulent state as the Reynolds number increases. A turbulent flow can improve the fluid's mixing within the channel. This can help disperse heat more evenly and stop stagnant regions from forming. The highest enhancement ratio was obtained in BR = 0.10 using TiO_2–SiO_2/Water-EG nanofluid followed by BR = 0.15 using the same fluid. This indicates the effect of nanofluid along with the blockage ratio. Furthermore TiO_2–SiO_2/Water-EG in BR = 0.10 possesses highest friction ratio. The lowest friction ratio and enhancement ratio was obtained by BR = 0.25 for using water as working fluid. There is an abrupt change of 56.70% in enhancement ratio for using hybrid nanofluid over single nanofluid for BR = 0.10 at Re = 20,000. Similarly, there is an increment in enhancement ratio of 18.13% for using BR = 0.10 over BR = 0.25 for the same nanofluid.

Fig. 27(b) indicates the Performance Evaluation Criterion for different nanofluid along with three different blockage ratios. The highest value was observed in BR = 0.10 using TiO_2–SiO_2/Water-EG nanofluid due to a higher enhancement ratio and friction ratio. The lowest value was obtained for CuO/water. When comparing the PEC value of hybrid and single nanofluids, the hybrid performs better because of its increased thermal conductivity. Change in blockage ratio has a greater impact in the heat transfer characteristics along with a high change due to using hybrid nanofluid.

6. Conclusion

The influence of different blockage ratios in the curved corrugated channels is investigated in this research. Furthermore, the assessment includes the evaluation of HT, pressure drop, and fluid flow characteristics. Principally, this numerical investigation aims to show that, to achieve the best possible thermal performance, it could be beneficial to incorporate both hybrid and single nanofluids into corrugated channels. This would simplify the design process and make heat exchangers more compact. Moreover, other findings from this investigation consist of the following.

- Using E-shaped baffles and trapezoidal-shaped corrugations improved the channel's thermal-hydraulic performance by increasing flow turbulence, causing vortex flow to occur, and breaking down the boundary layer. When compared to a smooth channel and a channel with merely corrugations, the usage of a curved corrugated channel with baffles produced higher thermal hydraulic properties. This can be explained by the increased turbulence and vortex generation caused by the baffles.
- For Re = 25,000 using curved corrugated channel with BR = 0.15, the HTC and *Nu* has increased by 39.77% and 62.12% respectively for using (20% TiO_2-80% SiO_2)/(60% Water- 40% EG) hybrid nanofluid over water. For the same hybrid nanofluid there is an increment of 18.71% in HTC for BR = 0.10 as opposed to BR = 0.25 at Re = 25,000. Using a higher volume fraction of nanofluid can enhance the *Nu* by approximately 10.26% for VF = 1%–5%.
- Implementation of hybrid nanofluid causes a drastic change in the pressure drop causing better mixing of fluid and high heat transfer. Pressure drop at smooth pipe is 10.21 Pa which turns into 1458.50 Pa due to the usage of trapezoidal shaped corrugation and E shaped baffles of blockage ratio 0.10. There is an increment of 48.44% for using BR = 0.10 over BR = 0.25 for ΔP.
- Considering the impact of hybrid nanofluid, a greater magnitude of PEC has been obtained by implementing (20% TiO_2-80% SiO_2)/(60% Water- 40% EG) hybrid nanofluid using BR = 0.10. Increasing the Re causes the PEC to increase. Optimum enhancement ratio and friction ratio has been found for the same configuration having a magnitude of 6.68 and 2.68 respectively. PEC increased by 36.49% for using BR = 0.10 over BR = 0.25.
- Thermodynamic characteristics of nanofluids can be investigated by measuring the Energy Ratio (ER), which is a measure of thermal energy conversion to mechanical energy.

In the field of industrial applications utilizing curved channels, it is widely anticipated that the integration of corrugation, baffles, and hybrid nanofluids would serve as a proficient passive approach in facilitating a thermal system with superior performance. The utilization of hybrid nanofluid offers several drawbacks, including its high cost and inherent stability issues. However, it represents a promising advancement in the quest for optimal cooling methods and the resolution of cooling challenges arising from the miniaturization of electronic devices.

Data availability statement

The model was initially validated by the authors using a computational and experimental reference model's data. A dataset based on several hydro-thermal parameters has subsequently been generated. The authors will make this dataset available upon request if it turns out to be helpful for upcoming projects related to this field.

CRediT authorship contribution statement

Rifat Ahamed: Writing – original draft, Visualization, Validation, Software, Methodology, Investigation, Formal analysis, Data curation, Conceptualization. **Musfequs Salehin:** Writing – original draft, Supervision, Project administration, Conceptualization. **M Monjurul Ehsan:** Writing – review & editing, Supervision, Project administration, Conceptualization.

Declaration of competing interest

The authors declare that they have no known competing financial interests or personal relationships that could have appeared to influence the work reported in this paper.

References

[1] R.K. Ajeel, K. Sopian, R. Zulkifli, A novel curved-corrugated channel model: thermal-hydraulic performance and design parameters with nanofluid, Int. Commun. Heat Mass Tran. 120 (2021), https://doi.org/10.1016/j.icheatmasstransfer.2020.105037.

[2] P. Naphon, Heat transfer characteristics and pressure drop in channel with V corrugated upper and lower plates, Energy Convers. Manag. 48 (2007) 1516–1524, https://doi.org/10.1016/j.enconman.2006.11.020.

[3] R.K. Ajeel, W.S.-I.W. Salim, K. Hasnan, Numerical investigations of heat transfer enhancement in a house shaped-corrugated channel: combination of nanofluid and geometrical parameters, Therm. Sci. Eng. Prog. 17 (2020) 100376, https://doi.org/10.1016/j.tsep.2019.100376.

[4] R. Dormohammadi, M. Farzaneh-Gord, A. Ebrahimi-Moghadam, M.H. Ahmadi, Heat transfer and entropy generation of the nanofluid flow inside sinusoidal wavy channels, J. Mol. Liq. 269 (2018) 229–240, https://doi.org/10.1016/j.molliq.2018.07.119.

[5] D. Sahel, H. Ameur, R. Benzeguir, Y. Kamla, Enhancement of heat transfer in a rectangular channel with perforated baffles, Appl. Therm. Eng. 101 (2016) 156–164, https://doi.org/10.1016/j.applthermaleng.2016.02.136.

[6] J.C. Maxwell, A Treatise on Electricity and Magnetism, Cambridge University Press, 2010, https://doi.org/10.1017/CBO9780511709340.

[7] A.M. Alklaibi, L.S. Sundar, A.C.M. Sousa, Experimental analysis of exergy efficiency and entropy generation of diamond/water nanofluids flow in a thermosyphon flat plate solar collector, Int. Commun. Heat Mass Tran. 120 (2021) 105057, https://doi.org/10.1016/j.icheatmasstransfer.2020.105057.

[8] L.S. Sundar, B. Mathew, A. Sefelnasr, M. Sherif, A.C.M. Sousa, Second law of thermodynamic analysis of 40:60% propylene glycol and water mixture based nanodiamond nanofluid under transition flow, Diam. Relat. Mater. 117 (2021) 108480, https://doi.org/10.1016/j.diamond.2021.108480.

[9] A.R. Sajadi, M.H. Kazemi, Investigation of turbulent convective heat transfer and pressure drop of TiO2/water nanofluid in circular tube, Int. Commun. Heat Mass Tran. 38 (2011) 1474–1478, https://doi.org/10.1016/j.icheatmasstransfer.2011.07.007.

[10] S. Zeinali Heris, M. Nasr Esfahany, S.G. Etemad, Experimental investigation of convective heat transfer of Al2O3/water nanofluid in circular tube, Int. J. Heat Fluid Flow 28 (2007) 203–210, https://doi.org/10.1016/j.ijheatfluidflow.2006.05.001.

[11] M. Awais, N. Ullah, J. Ahmad, F. Sikandar, M.M. Ehsan, S. Salehin, A.A. Bhuiyan, Heat transfer and pressure drop performance of Nanofluid: a state-of- the-art review, International Journal of Thermofluids 9 (2021) 100065, https://doi.org/10.1016/j.ijft.2021.100065.

[12] B. Saleh, L. Syam Sundar, Thermal performance, embodied energy and environmental CO2 emissions analyses for double pipe U-bend heat exchanger working with MWCNT/water nanofluid, Int. J. Therm. Sci. 169 (2021) 107094, https://doi.org/10.1016/j.ijthermalsci.2021.107094.

[13] B. Saleh, L.S. Sundar, Experimental study on heat transfer, friction factor, entropy and exergy efficiency analyses of a corrugated plate heat exchanger using Ni/water nanofluids, Int. J. Therm. Sci. 165 (2021) 106935, https://doi.org/10.1016/j.ijthermalsci.2021.106935.

[14] M. Khoshvaght-Aliabadi, A. Zamzamian, F. Hormozi, Wavy channel and different nanofluids effects on performance of plate-fin heat exchangers, J. Thermophys. Heat Tran. 28 (2014) 474–484, https://doi.org/10.2514/1.T4209.

[15] S. Noor, M.M. Ehsan, M.S. Mayeed, A.K.M.S. Islam, Study of convective heat transfer for turbulent flow of nanofluids through corrugated channels, in: Volume 8A: Heat Transfer and Thermal Engineering, American Society of Mechanical Engineers, 2014, https://doi.org/10.1115/IMECE2014-39061.

[16] D. Wen, Y. Ding, Experimental investigation into convective heat transfer of nanofluids at the entrance region under laminar flow conditions, Int. J. Heat Mass Tran. 47 (2004) 5181–5188, https://doi.org/10.1016/j.ijheatmasstransfer.2004.07.012.

[17] F. Ahmad, S. Mahmud, M.M. Ehsan, M. Salehin, Numerical assessment of nanofluids in corrugated minichannels: flow phenomenon and advanced thermo-hydrodynamic analysis, International Journal of Thermofluids 20 (2023) 100449, https://doi.org/10.1016/j.ijft.2023.100449.

[18] A. Akbarinia, R. Laur, Investigating the diameter of solid particles effects on a laminar nanofluid flow in a curved tube using a two phase approach, Int. J. Heat Fluid Flow 30 (2009) 706–714, https://doi.org/10.1016/j.ijheatfluidflow.2009.03.002.

[19] M. Monjurul Ehsan, M. Salehin, A.K.M.S. Islam, Investigation of thermal and hydrodynamic behaviour of Al2O3-water nanofluid through a rough parallel plate, Int. J. Automot. Mech. Eng. 14 (2017) 4432–4447, https://doi.org/10.15282/ijame.14.3.2017.4.0351.

[20] K. Scott, J. Lobato, Mass transport in cross-corrugated membranes and the influence of TiO 2 for separation processes, Ind. Eng. Chem. Res. 42 (2003) 5697–5701, https://doi.org/10.1021/ie030374b.

[21] R.K. Ajeel, W.S.-I.W. Salim, K. Hasnan, Thermal and hydraulic characteristics of turbulent nanofluids flow in trapezoidal-corrugated channel: symmetry and zigzag shaped, Case Stud. Therm. Eng. 12 (2018) 620–635, https://doi.org/10.1016/j.csite.2018.08.002.

[22] R.K. Ajeel, W.S.I.W. Salim, K. Hasnan, Influences of geometrical parameters on the heat transfer characteristics through symmetry trapezoidal-corrugated channel using SiO 2 -water nanofluid, Int. Commun. Heat Mass Tran. 101 (2019) 1–9, https://doi.org/10.1016/j.icheatmasstransfer.2018.12.016.

[23] M.K. Abdolbaqi, C.S.N. Azwadi, R. Mamat, W.H. Azmi, G. Najafi, Nanofluids heat transfer enhancement through straight channel under turbulent flow, Int. J. Automot. Mech. Eng. 11 (2015) 2294–2305, https://doi.org/10.15282/ijame.11.2015.12.0193.

[24] M. Monjurul Ehsan, S. Noor, S. Salehin, A.K.M. Sadrul Islam, Application of nanofluid in heat exchangers for energy savings, in: Thermofluid Modeling for Energy Efficiency Applications, Elsevier, 2016, pp. 73–101, https://doi.org/10.1016/B978-0-12-802397-6.00004-X.

[25] S. Noor, M.M. Ehsan, M.S. Mayeed, A.K.M.S. Islam, Convective heat transfer and pumping power requirement using nanofluid for the flow through corrugated channel, in: Volume 8A: Heat Transfer and Thermal Engineering, American Society of Mechanical Engineers, 2015, https://doi.org/10.1115/IMECE2015-52019.

[26] A.K. Santra, S. Sen, N. Chakraborty, Study of heat transfer due to laminar flow of copper-water nanofluid through two isothermally heated parallel plates, Int. J. Therm. Sci. 48 (2009) 391–400, https://doi.org/10.1016/j.ijthermalsci.2008.10.004.

[27] M. Bahiraei, S.M. Majd, Prediction of entropy generation for nanofluid flow through a triangular minichannel using neural network, Adv. Powder Technol. 27 (2016) 673–683, https://doi.org/10.1016/j.apt.2016.02.024.

[28] M.E. Nakhchi, J.A. Esfahani, Numerical investigation of turbulent Cu-water nanofluid in heat exchanger tube equipped with perforated conical rings, Adv. Powder Technol. 30 (2019) 1338–1347, https://doi.org/10.1016/j.apt.2019.04.009.

[29] Y. Xuan, Q. Li, Investigation on convective heat transfer and flow features of nanofluids, J. Heat Tran. 125 (2003) 151–155, https://doi.org/10.1115/1.1532008.

[30] O. Manca, S. Nardini, D. Ricci, A numerical study of nanofluid forced convection in ribbed channels, Appl. Therm. Eng. 37 (2012) 280–292, https://doi.org/10.1016/j.applthermaleng.2011.11.030.

[31] H.A. Mohammed, A.N. Al-Shamani, J.M. Sheriff, Thermal and hydraulic characteristics of turbulent nanofluids flow in a rib-groove channel, Int. Commun. Heat Mass Tran. 39 (2012) 1584–1594, https://doi.org/10.1016/j.icheatmasstransfer.2012.10.020.

[32] M. Awais, M. Saad, H. Ayaz, M.M. Ehsan, A.A. Bhuiyan, Computational assessment of Nano-particulate (Al2O3/Water) utilization for enhancement of heat transfer with varying straight section lengths in a serpentine tube heat exchanger, Therm. Sci. Eng. Prog. 20 (2020) 100521, https://doi.org/10.1016/j.tsep.2020.100521.
[33] K. Gasljevic, E.F. Matthys, Friction and heat transfer in drag-reducing surfactant solution flow through curved pipes and elbows, Eur. J. Mech. B Fluid 28 (2009) 641–650, https://doi.org/10.1016/j.euromechflu.2009.04.003.
[34] A. Noorani, G.K. El Khoury, P. Schlatter, Evolution of turbulence characteristics from straight to curved pipes, Int. J. Heat Fluid Flow 41 (2013) 16–26, https://doi.org/10.1016/j.ijheatfluidflow.2013.03.005.
[35] R. Yang, F.P. Chiang, An experimental heat transfer study for periodically varying-curvature curved-pipe, Int. J. Heat Mass Tran. 45 (2002) 3199–3204, https://doi.org/10.1016/S0017-9310(02)00023-6.
[36] P. Sriromreun, C. Thianpong, P. Promvonge, Experimental and numerical study on heat transfer enhancement in a channel with Z-shaped baffles, Int. Commun. Heat Mass Tran. 39 (2012) 945–952, https://doi.org/10.1016/j.icheatmasstransfer.2012.05.016.
[37] P. Promvonge, W. Jedsadaratanachai, S. Kwankaomeng, Numerical study of laminar flow and heat transfer in square channel with 30° inline angled baffle turbulators, Appl. Therm. Eng. 30 (2010) 1292–1303, https://doi.org/10.1016/j.applthermaleng.2010.02.014.
[38] S. Noor, M. Ehsan, S. Salehin, A.K.M.S. Islam, Heat Transfer and Pumping Power Using Nanofluid in a Corrugated Tube, 2014.
[39] K. Nanan, N. Piriyarungrod, C. Thianpong, K. Wongcharee, S. Eiamsa-ard, Numerical and experimental investigations of heat transfer enhancement in circular tubes with transverse twisted-baffles, Heat and Mass Transfer/Waerme- Und Stoffuebertragung 52 (2016) 2177–2192, https://doi.org/10.1007/s00231-015-1728-7.
[40] B. Lu, P.X. Jiang, Experimental and numerical investigation of convection heat transfer in a rectangular channel with angled ribs, Exp. Therm. Fluid Sci. 30 (2006) 513–521, https://doi.org/10.1016/j.expthermflusci.2005.09.007.
[41] R. Kamali, A.R. Binesh, The importance of rib shape effects on the local heat transfer and flow friction characteristics of square ducts with ribbed internal surfaces, Int. Commun. Heat Mass Tran. 35 (2008) 1032–1040, https://doi.org/10.1016/j.icheatmasstransfer.2008.04.012.
[42] F. Ahmad, S. Mahmud, M.M. Ehsan, M. Salehin, Thermo-hydrodynamic performance evaluation of double-dimpled corrugated tube using single and hybrid nanofluids, International Journal of Thermofluids 17 (2023) 100283, https://doi.org/10.1016/j.ijft.2023.100283.
[43] W. Jian, Y. Huizhu, S. Wang, S. Xu, X. Yulan, H. Tuo, Numerical investigation on baffle configuration improvement of the heat exchanger with helical baffles, Energy Convers. Manag. 89 (2015) 438–448, https://doi.org/10.1016/j.enconman.2014.09.059.
[44] P. Bichkar, O. Dandgaval, P. Dalvi, R. Godase, T. Dey, Study of shell and tube heat exchanger with the effect of types of baffles, Procedia Manuf. 20 (2018) 195–200, https://doi.org/10.1016/j.promfg.2018.02.028.
[45] H.A. Hussein, Numerical hydrothermal evaluation of heat transfer in a multi-mini-channel heat sink: effect of square pin fins, Results in Engineering 20 (2023) 101403, https://doi.org/10.1016/j.rineng.2023.101403.
[46] Z. Iqbal, K.S. Syed, M. Ishaq, Fin design for conjugate heat transfer optimization in double pipe, Int. J. Therm. Sci. 94 (2015) 242–258, https://doi.org/10.1016/j.ijthermalsci.2015.03.011.
[47] C. Gao, Z. Liu, Y. Qiu, K. Zhao, Modelling of geometric features of Micro-Channel made using abrasive assisted electrochemical Jet machining, Int. J. Electrochem. Sci. 15 (2020) 94–108, https://doi.org/10.20964/2020.01.24.
[48] K.-S. Yun, E. Yoon, Fabrication of complex multilevel microchannels in PDMS by using three-dimensional photoresist masters, Lab Chip 8 (2008) 245–250, https://doi.org/10.1039/B712932G.
[49] M. Awais, A.A. Bhuiyan, S. Salehin, M.M. Ehsan, B. Khan, MdH. Rahman, Synthesis, heat transport mechanisms and thermophysical properties of nanofluids: a critical overview, International Journal of Thermofluids 10 (2021) 100086, https://doi.org/10.1016/j.ijft.2021.100086.
[50] A. Bhattacharya, V. V Calmidi, R.L. Mahajan, Thermophysical properties of high porosity metal foams, n.d. www.elsevier.com/locate/ijhmt.
[51] S.K. Das, N. Putra, P. Thiesen, W. Roetzel, Temperature dependence of thermal conductivity enhancement for nanofluids, J. Heat Tran. 125 (2003) 567–574, https://doi.org/10.1115/1.1571080.
[52] T. Theres Baby, R. Sundara, Surfactant free magnetic nanofluids based on core-shell type nanoparticle decorated multiwalled carbon nanotubes, J. Appl. Phys. 110 (2011), https://doi.org/10.1063/1.3642974.
[53] R. Vinoth, B. Sachuthananthan, A. Vadivel, S. Balakrishnan, A.G.S. Raj, Heat transfer enhancement in oblique finned curved microchannel using hybrid nanofluid, Int. J. Therm. Sci. 183 (2023) 107848, https://doi.org/10.1016/j.ijthermalsci.2022.107848.
[54] L. Syam Sundar, E. Venkata Ramana, M.K. Singh, A.C.M. Sousa, Thermal conductivity and viscosity of stabilized ethylene glycol and water mixture Al2O3 nanofluids for heat transfer applications: an experimental study, Int. Commun. Heat Mass Tran. 56 (2014) 86–95, https://doi.org/10.1016/j.icheatmasstransfer.2014.06.009.
[55] H.K. Pazarlıoğlu, R. Ekiciler, K. Arslan, N. Adil Mohammed Mohammed, Exergetic, Energetic, and entropy production evaluations of parabolic trough collector retrofitted with elliptical dimpled receiver tube filled with hybrid nanofluid, Appl. Therm. Eng. 223 (2023) 120004, https://doi.org/10.1016/j.applthermaleng.2023.120004.
[56] O. Soltani, M. Akbari, Effects of temperature and particles concentration on the dynamic viscosity of MgO-MWCNT/ethylene glycol hybrid nanofluid: experimental study, Physica E Low Dimens Syst Nanostruct 84 (2016) 564–570, https://doi.org/10.1016/j.physe.2016.06.015.
[57] G.M. Moldoveanu, A.A. Minea, M. Iacob, C. Ibanescu, M. Danu, Experimental study on viscosity of stabilized Al2O3, TiO2 nanofluids and their hybrid, Thermochim. Acta 659 (2018) 203–212, https://doi.org/10.1016/j.tca.2017.12.008.
[58] P. Selvakumar, S. Suresh, Use of Al 2 O 3-Cu/water hybrid nanofluid in an electronic heat sink, IEEE Trans. Compon. Packag. Manuf. Technol. 2 (2012) 1600–1607, https://doi.org/10.1109/TCPMT.2012.2211018.
[59] H. Waqas, U. Farooq, A. Hassan, D. Liu, S. Noreen, R. Makki, M. Imran, M.R. Ali, Numerical and Computational simulation of blood flow on hybrid nanofluid with heat transfer through a stenotic artery: silver and gold nanoparticles, Results Phys. 44 (2023) 106152, https://doi.org/10.1016/j.rinp.2022.106152.
[60] R. Ekiciler, Analysis and evaluation of the effects of uniform and non-uniform wall corrugation in a pipe filled with ternary hybrid nanofluid, Arabian J. Sci. Eng. 49 (2024) 2681–2694, https://doi.org/10.1007/s13369-023-08459-4.
[61] J.E. Hesselgreaves, R. Law, D.A. Reay, Surface types and correlations, in: Compact Heat Exchangers, Elsevier, 2017, pp. 221–274, https://doi.org/10.1016/B978-0-08-100305-3.00006-9.
[62] E. Shashi Menon, Fluid flow in pipes, in: Transmission Pipeline Calculations and Simulations Manual, Elsevier, 2015, pp. 149–234, https://doi.org/10.1016/B978-1-85617-830-3.00005-5.
[63] Y. Zhang, Q. Li, H. Zhou, Heat transfer in fluidized beds, in: Theory and Calculation of Heat Transfer in Furnaces, Elsevier, 2016, pp. 101–129, https://doi.org/10.1016/B978-0-12-800966-6.00004-1.
[64] B. Choi, C. Kim, H. Kang, M.Y. Choi, General solutions of the heat equation, Phys. Stat. Mech. Appl. 539 (2020) 122914, https://doi.org/10.1016/j.physa.2019.122914.
[65] G. Towler, R. Sinnott, Design of reactors and mixers, in: Chemical Engineering Design, Elsevier, 2013, pp. 631–751, https://doi.org/10.1016/B978-0-08-096659-5.00015-8.
[66] M.Z. Rahman, M. Hasanuzzaman, Solar drying system, in: Technologies for Solar Thermal Energy, Elsevier, 2022, pp. 237–266, https://doi.org/10.1016/B978-0-12-823959-9.00010-6.
[67] A. Cavallini, Heat transfer and heat exchangers, in: Organic Rankine Cycle (ORC) Power Systems, Elsevier, 2017, pp. 397–470, https://doi.org/10.1016/B978-0-08-100510-1.00013-2.
[68] V. Zimparov, Extended performance evaluation criteria for enhanced heat transfer surfaces: heat transfer through ducts with constant wall temperature, Int. J. Heat Mass Tran. 43 (2000) 3137–3155, https://doi.org/10.1016/S0017-9310(99)00317-8.
[69] R.S. Vajjha, D.K. Das, B.M. Mahagaonkar, Density measurement of different nanofluids and their comparison with theory, Petrol. Sci. Technol. 27 (2009) 612–624, https://doi.org/10.1080/10916460701857714.

[70] B.C. Pak, Y.I. Cho, Hydrodynamic and heat transfer study of dispersed fluids with submicron metallic oxide particles, Exp. Heat Tran. 11 (1998) 151–170, https://doi.org/10.1080/08916159808946559.
[71] B. Takabi, H. Shokouhmand, Effects of Al2O3-Cu/water hybrid nanofluid on heat transfer and flow characteristics in turbulent regime, Int. J. Mod. Phys. C 26 (2015), https://doi.org/10.1142/S0129183115500473.
[72] U. Rea, T. McKrell, L. wen Hu, J. Buongiorno, Laminar convective heat transfer and viscous pressure loss of alumina-water and zirconia-water nanofluids, Int. J. Heat Mass Tran. 52 (2009) 2042–2048, https://doi.org/10.1016/j.ijheatmasstransfer.2008.10.025.
[73] Y. Xuan, W. Roetzel, Conceptions for heat transfer correlation of nano¯uids, n.d. www.elsevier.com/locate/ijhmt.
[74] H.C. Brinkman, The viscosity of concentrated suspensions and solutions, J. Chem. Phys. 20 (1952) 571, https://doi.org/10.1063/1.1700493.
[75] T. Hayat, S. Nadeem, Heat transfer enhancement with Ag–CuO/water hybrid nanofluid, Results Phys. 7 (2017) 2317–2324, https://doi.org/10.1016/j.rinp.2017.06.034.
[76] R.L. Hamilton, O.K. Crosser, Thermal conductivity of heterogeneous two-component systems, Ind. Eng. Chem. Fundam. 1 (1962) 187–191, https://doi.org/10.1021/i160003a005.
[77] M.Z. Saghir, M.M. Rahman, Forced convection of Al2O3-Cu, TiO2-SiO2, FWCNT- Fe3O4, and ND-Fe3O4 hybrid nanofluid in porous media, Energies 13 (2020), https://doi.org/10.3390/en13112902.
[78] H. Hausen, Neue Gleichungen Fur die Warmeubertragung bei freier oder erzwungener Stromung, Allg, Waerme 9 (1959) 75–79. https://cir.nii.ac.jp/crid/1571135650095918336.bib?lang=en. (Accessed 16 August 2023).
[79] V. Gnielinski, New equations for heat and mass transfer in the turbulent flow in pipes and channels, NASA STI/Recon Technical Report A 41 (1975) 8–16.
[80] Fluid_Mechanics, (n.d.)..
[81] B.S. Petukhov, V.N. Popov, THEORETICAL CALCULATION OF HEAT TRANSFER AND FRICTIONAL RESISTANCE FOR TURBULENT FLOW IN A TUBE OF EQUILIBRIUM DISSOCIATING HYDROGEN (T), 2, 1964. https://www.osti.gov/biblio/4591807.
[82] W. Yu, D.M. France, E.V. Timofeeva, D. Singh, J.L. Routbort, Comparative review of turbulent heat transfer of nanofluids, Int. J. Heat Mass Tran. 55 (2012) 5380–5396, https://doi.org/10.1016/j.ijheatmasstransfer.2012.06.034.
[83] R.S. Vajjha, D.K. Das, A review and analysis on influence of temperature and concentration of nanofluids on thermophysical properties, heat transfer and pumping power, Int. J. Heat Mass Tran. 55 (2012) 4063–4078, https://doi.org/10.1016/j.ijheatmasstransfer.2012.03.048.